Mass Loss in Parabolic Collisions between Giant Stars and Stellar Mass Black Holes

By

Joseph Friedman

Department of Physics

Allegheny College

Meadville, Pennslyvania

April, 2023

Submitted in fulfillment of the senior thesis requirements of the
Department of Physics at Allegheny College
and approved by the senior thesis committee.

Dr. Jamie Lombardi	**Date**	**Dr. Daniel Willey**	**Date**

Pledge

Acknowledgments

First I would like to thank my mother for encouraging me to pursue my passions. Without her love and support, I never would have made it this far. Next, I would like to thank my advisor Dr. Jamie Lombardi for the guidance and encouragement that he gave me throughout my time at Allegheny. I am quick to tell any who asks that if it were not for Lombardi I would have never attended Allegheny in the first place. Additionally, I would like to thank Fulya Kiroglu for providing me with information from her research with cluster simulations, without which this project would never have been done. Lastly, I would like to thank Jason Jeannette. While he may have had less of an impact on my life since leaving Nashville for college, I would not be the person that I am today without him. Thank you for showing me a path with heart.

Name: Joseph Friedman Student Date: April, 2023

Major: Physics

Thesis Committee: Dr. Jamie Lombardi, Dr. Daniel Willey

Title: Mass Loss in Parabolic Collisions between Giant Stars and Stellar Mass Black Holes

Abstract

In globular clusters stars and stellar mass black holes interact with each other. This project examines the types of interactions that occur in globular clusters by using MESA to evolve a giant star and using the SPH code Starsmasher to simulate several such interactions between a 10M red giant star and black holes of various masses. By comparing the results of these simulations to those of Kiroglu et al. 2022, I find that interactions between giant stars and black holes do not follow the same relationship as those involving main sequence stars and black holes.

1. Introduction/Background

All across the world, people look into the sky and see a bright red dot in the constellation of Orion. That dot is the star Betelgeuse, a red giant star and one of the brightest stars in the night sky. If Betelgeuse were put in the place of the Sun, its outer edge would extend past the asteroid belt. The incredible size of red giants makes them more likely to interact with other astronomical objects. These interactions create phenomena such as gravitational waves that may become observable in the future as more sensitive gravitational wave detectors like the Laser Interferometer Space Antenna (LISA) come into being. Additionally, the mass bound to the black hole in these interactions creates electromagnetic radiation which can be detected with with tools like the James Webb Space Telescope. However, due to the vast distances involved, it is difficult to tell what is going on in these interactions. This project aims to simulate this type of interaction using the program Starsmasher and the Modules for Experiments in Stellar Astrophysics (MESA) to learn more about how massive objects interact.

1.1 Stars

Stars are massive clouds of gas held together by gravity with enough internal pressure and temperature to sustain nuclear fusion. Stars are composed mostly of hydrogen and helium with trace amounts of heavier elements. The amount of heavier elements in a star is called its metalicity. Nuclear fusion is a process in which lighter elements combine into heavier elements. Over billions of years, as stars are born and die, the abundance of heavier elements increases. As such, stars formed more recently have larger quantities of heavier elements as the gas that formed the star had more of those elements. Fusion releases large amounts of energy which supports the star from collapsing due to gravity and releases light and heat. Hydrogen fusion requires less energy than fusing heavier elements and is the most abundant element in stars. While a star is solely fusing hydrogen into helium it is referred to as a main sequence (MS) star.

1.2 Red Giants

Red giants (RG) are the result of MS stars that have expended the hydrogen fuel in their cores but have not yet begun helium fusion. Hydrogen fusion in a shell around an inert helium core supports the star as the helium core expands. Eventually, the core contracts which causes the solar envelope to expand into the subgiant branch. As the envelope expands, a convective zone forms, and the star rapidly increases in radius as it climbs the red giant branch. The star's total luminosity increases due to the increased total surface area while the surface temperature decreases (Carroll and Ostlie 460). The net decrease in surface temperature and increase in radius gives this stage in a star’s life its characteristic color and size: hence the name red giant. The outer layer of RG stars is much less dense than that of MS stars and as such, they are less tightly bound to the star. This allows the outer layer of RGs to be stripped by gravitational interactions with other massive bodies (Alexander 2017) more easily than for MS stars. As the core collapses, temperature and pressure increase until helium fusion begins and the next stage of stellar evolution begins.

1.3 Black Holes

Black holes form when massive stars die. Specifically, massive stars undergo a supernova explosion, and the remnant of the star's core collapses. If the star has less than eight solar masses, the core will survive as a white dwarf. With a mass of between eight and twelve (or 15 depending on who you ask) solar masses, the core will be supported by neutron degeneracy pressure and form a neutron star. If the star is greater than 25 solar masses, the gravity of the collapsing core will overcome neutron degeneracy pressure and collapse to form a black hole (Carroll and Ostlie 534, Fogarty 1). Black holes are separated into three categories according to mass: stellar mass black holes (five to a hundred solar masses), intermediate-mass black holes or IMBH, (hundreds to thousands of solar masses), and supermassive black holes (millions to billions of solar masses).

The size of a BH is somewhat indistinct, so instead the size of a BH is typically described by the radius at which the escape velocity from the BH is equal to the speed of light (c = 299,792,458 m/s). This radius is called the Schwarzschild radius and is given by

$$Schwarzschild\ Radius = R_S = \frac{2GM}{c^2}, \qquad (1)$$

where M is the mass of the BH, c is the speed of light, G is the gravitational constant, and R_S is the Schwarzchild radius. For where this radius comes from, see Appendix 1. Black holes get their name because within the Schwarzschild radius no photons can pass information to the outside world, and as such the black hole appears black.

For this project, I want to know the mass of stellar mass BHs that are involved in tidal disruption events (TDEs). In Figure 1 below, the mass of BHs and stars involved in TDEs is shown for approximately 100 globular clusters (see section 1.5 for more details on globular clusters). From this Figure, it can be seen that the most common mass of BHs in TDEs is between ten and forty solar masses with only a few above eighty solar masses. Because of this, I will be using BHs of mass 10, 20, 40, and 80 solar masses for all of my simulations.

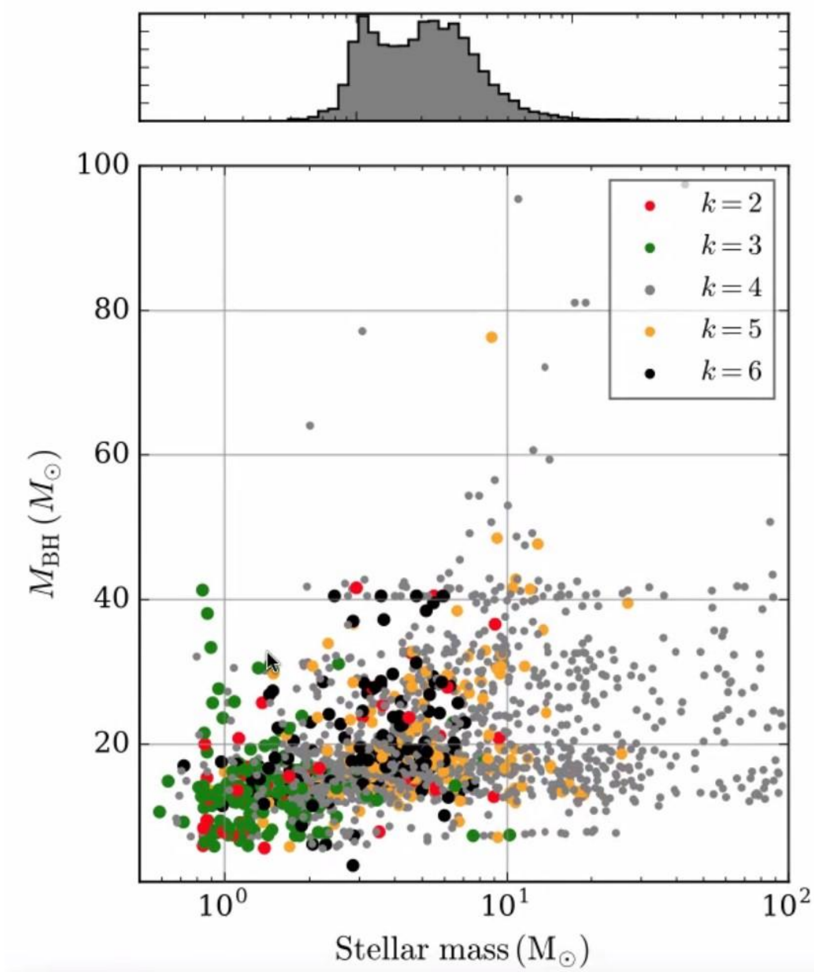

Figure 1: Mass of BH vs mass of star involved in TDEs. Data was collected from about 100 cluster simulations. (Kiroglu 2023)

1.4 Tidal Forces and the Tidal Radius

Tidal forces are forces caused by the difference in the gravitational force from one object on varying parts of another object. For example, in the Earth-Moon system, one side of the Earth is nearer to the Moon than the other. As we already know the force of gravity on an object scales proportionally to $\frac{1}{r^2}$, which causes the force of gravity from the Earth on the Moon to be stronger on the side of the Moon closer to Earth than that on the further side. To explore this further, consider a BH-star system. Let *r* be the separation between the BH and the center of the star, *R* be the radius of the star, M_* be the mass of the star, and M_{bh} be the mass of the BH.

The force of gravity between any two masses M and m is

$$F_g = \frac{GMm}{r^2}, \qquad (2)$$

where G is the gravitational constant $G = 6.67\times10^{-11}$ $m^3k^{-1}s^{-2}$. Plugging in the specifics for the BH and test mass gives

$$F_{gc} = \frac{GM_{bh}m_1}{r^2}.$$

Similarly, the force of gravity from the BH on the same test mass at the surface of the star closest to the BH is

$$F_{gs} = \frac{GM_{bh}m_1}{(r-R)^2}.$$

The difference between F_{gs} and F_{gc} is the tidal force, which expanded to lowest nonvanishing order equals

$$F_t = -2G\frac{RM_{bh}m_1}{r^3}. \qquad (3)$$

A significant distance in this work is the tidal radius which is the distance from the BH at which the tidal force is equal to the force of gravity from the star on a mass m_1 at the star's surface. This can be found by plugging $M = M_*$ into Equation 2 and setting the result equal to Equation 3:

$$F_t = \frac{2RGM_{bh}m_1}{r^3} = \frac{GM_*m_1}{R^2} = F_{g*},$$

where F_{g*} is the gravitational force from the star on a test mass on the surface. Simplifying this equation and solving for *r* gives the tidal radius yielding

$$r_t = R\sqrt[3]{\frac{M_{bh}}{M_*}}. \qquad (4)$$

The factor of 2 from Equation 3 is typically ignored hence its absence in Equation 4. Roughly, a star whose pericenter distance (the closest the star gets to the BH) is less than r_t is expected to be totally destroyed, one whose pericenter distance is between r_t and $2r_t$ is expected to be partially disrupted. One with a pericenter distance greater than $2r_t$ is expected not to be disrupted. The above statements are approximate rather than exact, but they provide a sanity check for my simulations to ensure that my results are reasonable.

1.5 Stars in Globular Clusters

Gravitational interactions between giant stars and stellar mass BH occur with some frequency in globular clusters. Globular clusters are collections of thousands to hundreds of thousands of stars that formed from the same gas cloud (Carroll and Ostlie 474). The velocities of most of the objects in a globular cluster relative to each other are quite low, usually on the order of 10-20 km/s. Using Cluster Monte Carlo simulations, Fulya Kıroğlu created Figures 2 and 3 below which show the mass of stars involved in TDEs compared to the time of the TDE and the radius of stars involved in TDEs compared to the mass of the star, respectively. Notice that most stars involved in TDEs are between one and five solar masses ($M_\odot$) with a small number of TDEs involving stars of ten $M_\odot$ or more. Additionally, many of the lower-mass stars involved in TDEs have a radius of around ten solar radii ($R_\odot$) and the higher-mass stars have larger radii, typically on the order of $100R_\odot$ or more.

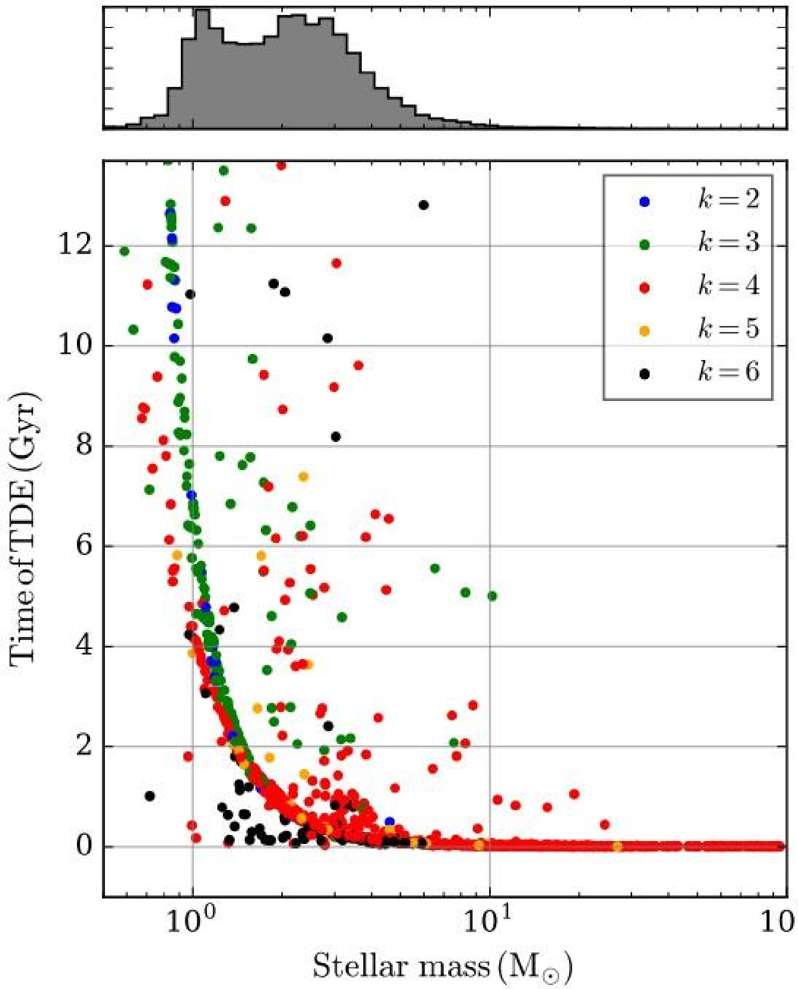

Figure 2: Mass of stars involved in tidal disruption events (TDEs) compared to the age of the cluster. Different colors represent different stages of stellar evolution as can be seen in Table 1 below. Data are collected from about 100 cluster simulations. (Kiroglu 2022)

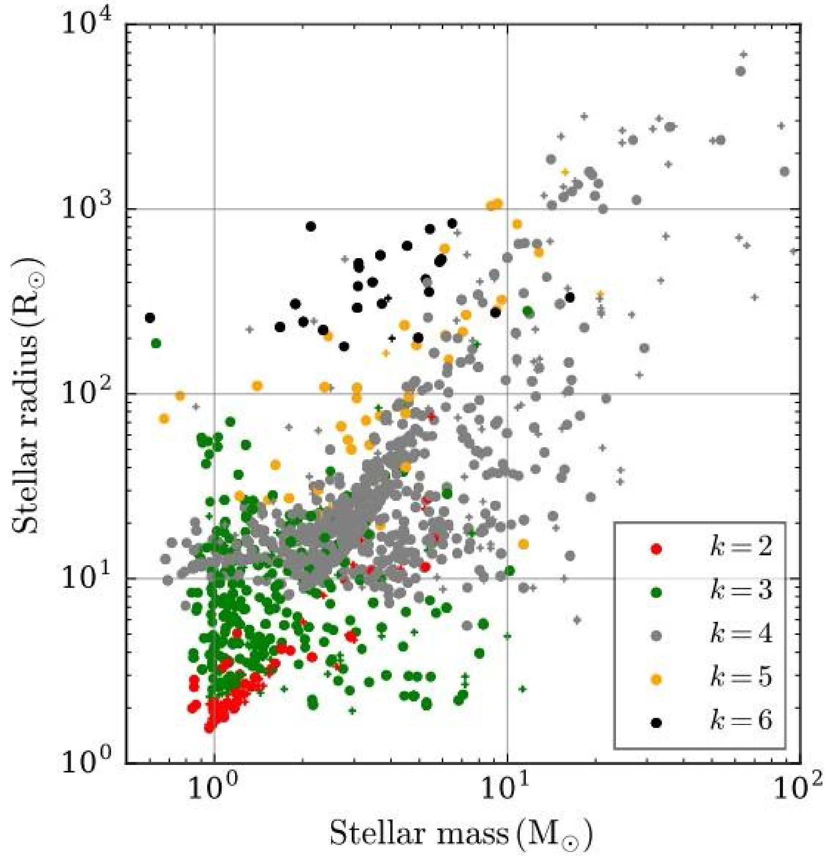

Figure 3: Mass of stars involved in TDEs compared to the radius of the star when the TDE occurred. Different colored dots represent different stages in stellar evolution as can be seen in Table 1 below. These data are collected from the same ~100 cluster simulations as Figure 1. (Kiroglu 2022)

Evolutionary State of the Star

kstar	evolutionary state
0	Main Sequence (MS), < 0.7 $M_\odot$
1	MS, > 0.7 $M_\odot$
2	Hertzsprung Gap
3	First Giant Branch
4	Core Helium Burning
5	Early Asymptotic Giant Branch (AGB)
6	Thermally Pulsing AGB

Table 1: Key for Cluster Simulations above. Each number corresponds to the color of the dots in Figures 2 and 3 above. Notice that the most common colors in Figures 2 and 3 correspond to k=3 for lower-mass stars and k=4 for higher masses, both of which are representative of stars in the giant stage of stellar evolution. (Kiroglu 2022)

1.6 Orbits

There are three types of orbits: elliptical, parabolic, and hyperbolic. In a hyperbolic orbit, the star will pass by the BH once and then escape the gravitational effects of the BH. In a parabolic orbit, the star has an initial velocity of zero at a distance of infinity and, in the point mass approximation, has just enough energy to escape the system. However, as the star passes the BH, the BH's gravity slows down the star which reduces the star's kinetic energy this can lead to the star becoming gravitationally bound to the BH. Elliptical orbits are any in which the star is bound to the BH and will continue to orbit indefinitely unless the star is destroyed or some outside force disrupts the orbit. An important point in an orbit is the periastron distance, the distance of closest approach between the star and BH. The periastron distancefor an ellipse is given by

$$r_p = a(1 - e),$$

where a is the semimajor axis of the ellipse and e is the eccentricity of the ellipse. The eccentricity of an ellipse is between zero and one with an eccentricity of zero corresponding to a circle and one corresponding to a parabola. A hyperbolic orbit has an eccentricity greater than one.

1.7 Common Envelope

A common envelope is a cloud of matter that is gravitationally bound to multiple objects. In other words, it is an envelope of material that is common to a set of objects, hence the name. In a collision between a star and BH some mass will be lost by the star. Some of this mass will become bound to the BH, some will be ejected from the system, and some will become part of the common envelope. Drag from the common envelope can contribute to orbital decay as a binary system evolves.

1.8 Prior Works

No study that I am aware of has examined stellar mass BH interactions with RG stars. Similar studies have been conducted with supermassive BHs and various stars (MacLeod et al. 2012), IMBH and MS stars (Kiroglu et al. 2022), and neutron stars with red giant stars (Lombardi et al. 2005). In general, giant stars are more likely to interact with other massive objects due to their larger radii. However, stars stay in the RG stage for much less time than the main sequence (MacLeod 2012). While the size and lifetime of giants work against each other, the net result is that giant stars still make up a significant portion of interactions between massive objects.

In their 2022 paper, Kiroglu, Lombardi, Kremer, and others use a relationship between the pericenter distance and the mass lost by the star after the first pass for MS-IMBH interactions given by

$$\beta^{-1} = \frac{r_p}{r_t} = \zeta^{1/3}\left(\frac{\rho_*}{\rho(R)}\right)^{1/3}. \quad (5)$$

Here, β^{-1} is the ratio of the pericenter distance r_p to the tidal radius r_t, a more useful value in comparing different stars than simply using the distance between the BH and star. The constant ζ is found experimentally by Kiroglu et al. to be ~5.6. The density of the star ρ_* is

$$\rho_* = \frac{3M_*}{4\pi R_*^3} \qquad (6)$$

$\rho(R)$ is the density of the star as a function of the radius R given by

$$\rho = \frac{3M(R)}{4\pi R^3}, \qquad (7)$$

where $M(R)$ is the mass within the radius R (Law-Smith et al. 2019; Ryu et al. 2020b). I will be comparing my results to this relationship and will calculate the value of ζ for each run to see if my results agree with those of Kiroglu et al. by solving Equation 5 for ζ which gives

$$\zeta = \left(\frac{r_p}{r_t}\right)^3 \frac{\rho(R)}{\rho^*}, \qquad (8)$$

In their 2012 paper, MacLeod et al. picked orbital paths such that the tidal radius of the core of a giant star was less than the pericenter distance which was smaller than the tidal radius of the star's envelope. This allowed them to say with reasonable certainty that the core of the star would be undisturbed and could focus on models that accurately describe the envelope of the star rather than the core. They also found that, within the boundary described above, there was always some amount of mass bound to the star after the collision. This stands in contrast to the findings of Guillochon & Ramirez-Ruiz who found that for collisions between main sequence stars and BH the star is totally disrupted in collisions with β ~ 1.9 or greater (2012).

2. Methodology

In this research, I model a RG using the stellar evolution code MESA, relax it in the hydrodynamics code Starsmasher, and simulate colliding it with a BH while varying the pericenter distance in order to find a relationship between the pericenter distance and the mass lost by the red giant. By examining Figures 1 and 2 above, I decided to model a $2M_\odot$ star with a radius of around $10R_\odot$ as well as a $10M_\odot$ star with a radius of around $100R_\odot$.

2.1 MESA

MESA is an open-source program used to evolve stars as they age. This program has been in use for over a decade and continuously improves as the community learns more about specific situations. Paxton et al. (2011) compared massive stars created using MESA to similarly sized stars created using other stellar evolution codes as can be seen in Table 2. An important thing to note from this table is that the MESA model provides data similar to the data from the other modeling programs.

Core Burning Element	Lifetime (years) HMM	WHW	LSC	MESA	
		$M_i = 15M_\odot$			
H	1.13	1.11	1.07	1.14	$\times 10^7$
He	1.34	1.97	1.4	1.25	$\times 10^6$
C	3.92	2.03	2.6	4.23	$\times 10^3$
Ne	3.08	0.732	2.00	3.61	
O	2.43	2.58	2.43	4.10	
Si	2.14	5.01	2.14	0.810	$\times 10^{-2}$
		$M_i = 20M_\odot$			
H	7.95	8.13	7.48	8.01	$\times 10^6$
He	8.75	11.7	9.3	8.10	$\times 10^5$
C	9.56	9.76	14.5	13.5	$\times 10^3$
Ne	0.193	0.599	1.46	0.916	
O	0.476	1.25	0.72	0.751	
Si	9.52	31.5	3.50	3.32	$\times 10^{-3}$
		$M_i = 25M_\odot$			
H	6.55	6.706	5.936	6.38	$\times 10^6$
He	6.85	8.395	6.85	6.30	$\times 10^5$
C	3.17	5.222	9.72	9.07	$\times 10^2$
Ne	0.882	0.891	0.77	0.202	
O	0.318	0.402	0.33	0.402	
Si	3.34	2.01	3.41	3.10	$\times 10^{-3}$

Table 2: Comparison of massive star lifespans from different methods including MESA. Included are the life spans of each core burning phase from hydrogen (H) to silicon (Si).

HMM–Hirschi et al. (2004); WHW– Woosley et al. (2002); LSC–Limongi et al. (2000); MESA-Paxton, Bill (2017)

MESA is especially useful as it contains many saved models that can be used as the base for new models of stars. These preset models fall into one of three categories: white dwarfs, pre-main sequence stars with very low mass, and zero-age main sequence (ZAMS) stars. MESA also contains information regarding expected values for density, pressure, and multiple other aspects of a star. The output from MESA takes the form of profile files that correspond to different times in the star's evolution. Each profile contains a plethora of information about the star that can be used to perform other calculations. MESA is an incredibly powerful tool for studying individual stars, but for studying how stellar objects interact, other tools are needed.

To simulate a collision between an RG and a BH, I must first create the RG model. To do this I use MESA to age a $10M_{\odot}$ star through the main sequence, up the red giant branch, and back down towards the asymptotic branch. I set the metallicity of this star to be 0.002 which is indicative of a star formed long ago or in a distant globular cluster. From this MESA run, I can select profile files from various times to use in Starsmasher. A Hertzsprung-Russell diagram, which shows the star's luminosity on the *y*-axis and surface temperature on the *x*-axis, of the $10M_{\odot}$ star can be seen in Figure 4 below. MESA does this by tracking things like the rate of nuclear fusion in the core of the star. During this process, MESA produces profile files at regular time intervals which can be used in Starsmasher runs as the initial state of the star. The orange dot in Figure 4 corresponds to the profile I use.

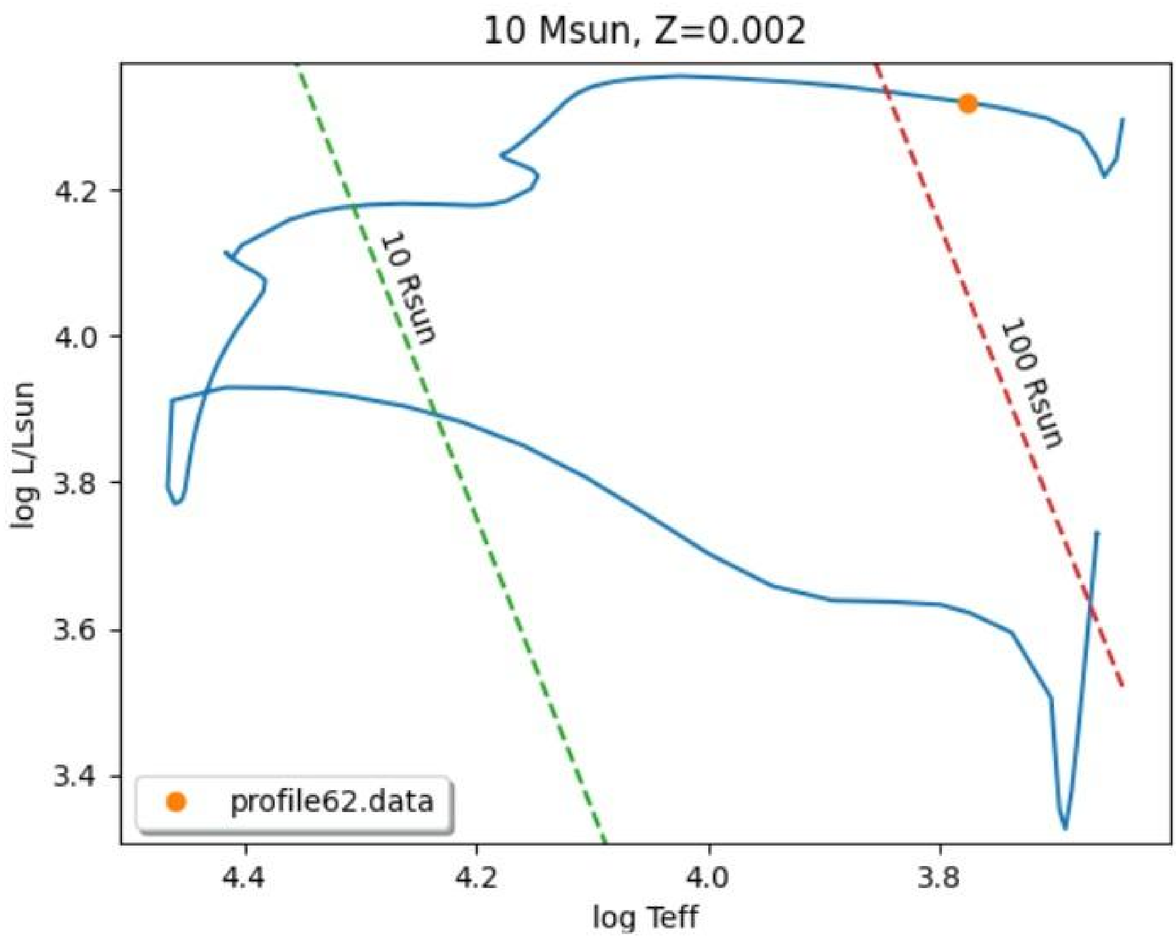

Figure 4: HR diagram of a $10M_{\odot}$ star as it evolves in MESA. The profile shown has a radius of $134.4R_{\odot}$ as that is the potential value of interest. This Figure and others with similar formatting were created using Hypermongo

2.2 Starsmasher

Starsmasher is a program that allows multiple objects to interact gravitationally and hydrodynamically. Starsmasher uses smoothed particle hydrodynamics (SPH) to simulate stars and other massive objects. SPH codes work by treating an object as a collection of particles that interact with each other through gravity and hydrodynamics. Each particle has properties such as mass, position, velocity, and composition and is represented as a kernel in which most of the particle's mass lies at the center and the remainder is distributed across the extent of the kernel

(Lombardi 2017). These kernels overlap with neighboring kernels. The data from a given point in the star are found from the combination of all of the kernels that overlap at that point. A defining characteristic of any kernel is its smoothing length *h* which is typically equal to half of the radius of the kernel but that can vary depending on the SPH code being used. A simple example kernel can be seen in Figure 5 with the kernel's central particle shown in red, the particles that affect the central particle in blue, and particles outside of the kernel (which do not hydrodynamically affect the central particle) in black. Each particle shown has its own kernel which looks similar to the one shown, and the properties of the star are found through the combination of every kernel in the area of interest.

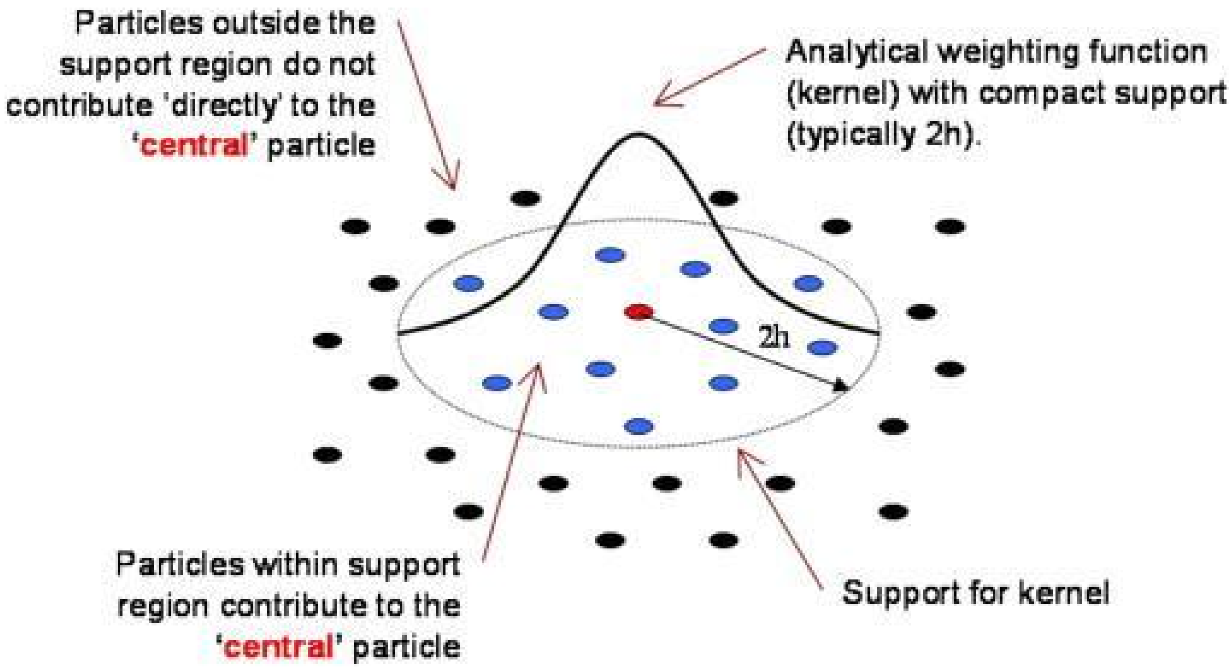

Figure 5: An example kernel. The central particle (red) is affected by the particles within its kernel (blue). The particles outside of the kernel do not contribute to the central particle (black). Karekal et al. (2011)

SPH codes like Starsmasher excel at tracking the physical properties that each particle possesses, this includes momentum and internal energy as well as others (Rosswog 2009). The internal properties tracked with SPH are what differentiate SPH simulations from N-body simulations which are better suited for larger-scale scenarios with more than several astronomical objects and treat each body as a single mass with gravitational but not hydrodynamic forces. If one wanted the benefits of both SPH and N-body simulations, an N-body code could be used to simulate a globular cluster, switch to using SPH when objects approach each other to provide the specific results of close encounters, then feed the results back into the N-body code once the objects have separated from each other and continue running.

An additional strength of Starsmasher is that dense objects can be included as point masses which can act gravitationally on particles without contributing to hydrodynamic effects. For example, both a black hole and the core of a red giant can be treated as point masses. This is necessary for red giants as the density gradient from the core of the star to the outer edge is so steep that it is difficult to model accurately. By using a point mass on the order of one to two solar masses as the core of a ten solar mass star, the remainder of the star covers a narrower range of densities by orders of magnitude (Lombardi 2017). Similarly, the black hole is treated as a point mass to simplify the simulation. This can lead to situations where the timestep of the simulation rapidly approaches zero as mass falls from the star onto the black hole. As the particles get crushed onto the BH the smoothing length *h*, and consequently the timestep, become vanishingly small. This problem can be addressed by setting a minimum value for *h* for each particle.

Starsmasher uses a set of units such that the unit of distance is $R_\odot$, the radius of the sun. The unit of mass is solar masses, $M_\odot$. Starsmasher also simplifies numbers by setting the value of the gravitational constant G equal to one. This system is sometimes abbreviated as

$$R_\odot = M_\odot = G = 1.$$

Time units in Starsmasher come from the only arrangement of $R_\odot$, $M_\odot$, and G that results in units of seconds. The constant G has units of $\frac{m^3}{kg*s^2}$, R is a distance and as such is in m, and M is a mass with units of kg. There is only one way to arrange these in order to get a time in seconds and that is

$$T = \sqrt{\frac{R_\odot^{\ 3}}{GM_\odot}} \approx 1600\ seconds \qquad (9)$$

Similarly, Starsmasher uses energy units from a combination of $R_\odot$, $M_\odot$, and G that gives units of joules. Specifically, one energy unit is given by

$$E = \frac{GM_{\odot}^{2}}{R_{\odot}} \approx 3.79 * 10^{41}\ joules$$

There are two types of Starsmasher simulations that matter to the topic at hand: relaxation runs and dynamic runs.

2.2.1 Relaxation Runs

A relaxation run is one in which there is only one object and its constituent particles are allowed to interact with each other to reach a hydrostatic equilibrium. This is necessary because when a star is generated, the particles are placed in a hexagonal close-packed lattice as can be seen on the left side of Figure 5 for a $10M_{\odot}$ giant star. A successful relaxation run can be seen on the right side of Figure 5 for the same star. Unfortunately, relaxing a RG is more complicated than a main sequence star. This is due to the massive pressure gradient that exists between the core of the RG and its outer layers. Additionally, a good relaxation should end with near zero kinetic energy. If considerable kinetic energy is present at the end of a relaxation run then the star is likely to be continuing to expand, a sign that either the star is not done relaxing or that it will continue to expand indefinitely. Solutions to situations such as these among others are discussed in the Starsmasher Specifics section below. Figure 5 and other Figures like it are created using Splash (Price 2007).

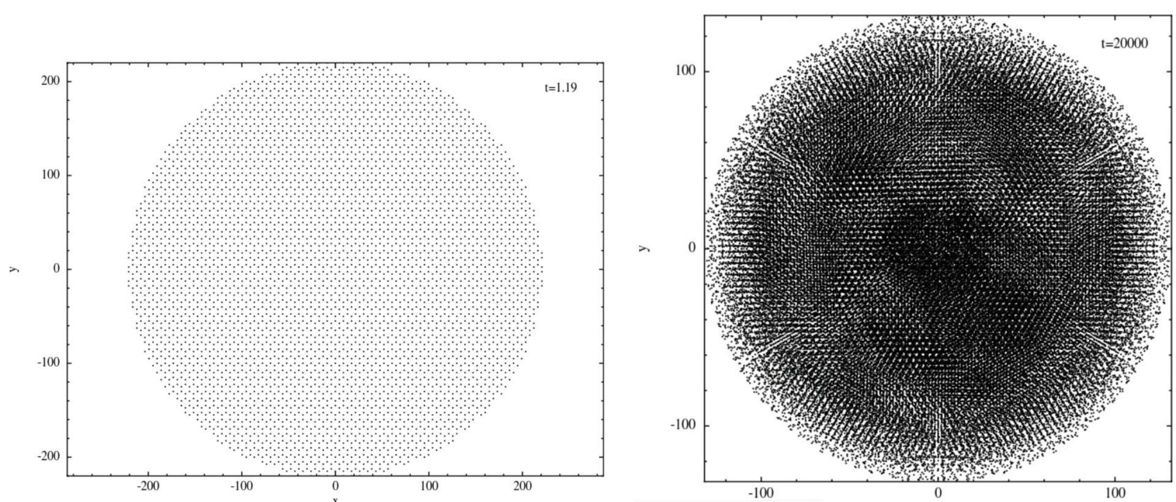

Figure 5: A nonrelaxed $10M_\odot$ star (left) compared to the same star post-relaxation run (right). In the nonrelaxed model, the particles are lined up in a hexagonal close-packed lattice. The axis use units of $R_\odot$ and the time units used are explained in the Starsmasher section.

2.2.2 Dynamical Run

A dynamical run includes multiple bodies, namely a BH in addition to the red giant. There are many parameters that I can adjust in the dynamical runs, but for the purposes of this project, I vary the pericenter distance and the mass of the BH across multiple runs to see how these affect the mass lost by the star. The other initial conditions I will keep constant so that any pattern that emerges can be accounted for by just the pericenter distance and BH mass. I choose to set the initial velocity of the star at infinity to be equal to zero which results in a parabolic trajectory. This approximation is appropriate as these interactions would be most commonly found in globular clusters in which the dispersion velocity is on the order of 10 km/s, significantly lower than the velocities that arise from the collision itself. Having this as the initial condition makes it clear whether or not the star loses significant energy during the first orbit because if it does lose energy the star will no longer be able to escape the system and will complete additional orbits around the BH. I will vary the pericenter distance from zero to $1.5r_t$ in order to observe a wide range TDEs. The limiting factor on the pericenter distance for these simulations is computational time. As the pericenter distance increases, the orbital period of the system increases which in turn requires more computational time for the same number of passages between the star and BH.

2.2.3 Starsmasher Specifics

For a given Starsmasher run, there are three input files of note: the stellar profile, init, and input files. Stellar profiles are created by MESA periodically throughout the evolution of a star. For some of my initial simulations, I used a profile in which the star was still in the subgiant stage of stellar evolution. For the remainder of my simulations, I will use a profile from later in the same evolution corresponding to when the star is on the red giant branch. The init file defines the type of simulation being run, whether relaxation or dynamical. The input file contains a multitude of variables that I am adjusting throughout the project. This includes things like the number of particles used to represent the star, N, as well as more involved values like equalmass and TRELAX which affect the mass assigned to particles and the drag force on the particles. This drag force has proven to be critical to my relaxation attempts so far as in my early attempts the star continuously expanded well past reasonable distances. This can be seen in Figure 6 below where a $10M_{\odot}$ RG expanded to a radius of $2000R_{\odot}$. By adjusting the value of TRELAX, I can vary the drag force as follows:

$$F_{drag} = -\frac{V}{T_{RELAX}}. \qquad (10)$$

As can be seen, the drag force on a particle is proportional to the velocity of the particle and inversely proportional to T_{RELAX}. Another variable of note is hfloor which sets a minimum value for the smoothing length in terms of solar radii. Setting an hfloor value helps prevent situations in which the smoothing length decreases drastically which in turn decreases the time step until the simulation is at an effective standstill. The value of hfloor needs to stay as small as possible to maintain accuracy in the simulation while still solving this problem.

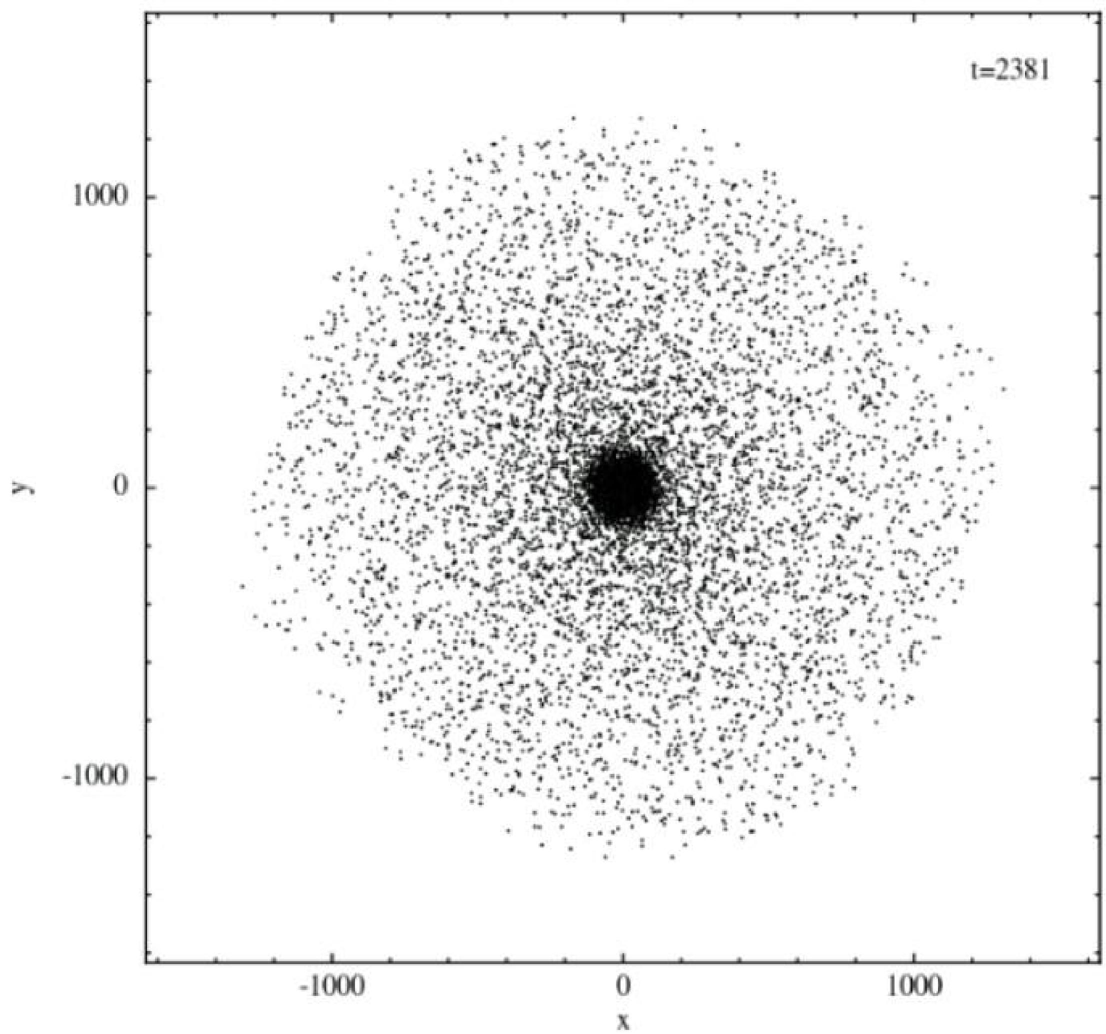

Figure 6. A failed relaxation attempt of a $10M_{\odot}$ RG star. The scale here is in units of solar radii. This attempt did not include the drag force introduced by the TRELAX variable, which restricts this expansion in later attempts.

2.2.4 Jump Runs

In dynamic runs in which the pericenter distance is greater than about 0.5 tidal radii the orbital period proves to be inconveniently long. After the first pass, the star's orbit remains highly elliptical, resulting in a long orbital period (on the order of thousands of years or longer). For the purpose of this project, what happens to the star during most of that orbit does not matter.

Therefore I set up runs that skip the star from one side of its orbit to the other when applicable. The determining factor in whether or not a jump can be used is the comparison between the star's thermal timescale and its orbital period. The thermal timescale is the amount of time it would take for a star to expend all of its gravitational energy at its current luminosity (Carroll and Ostlie 298). For the case of my $10M_\odot$ RG, the thermal timescale is on the order of thousands of years. For a derivation of this, see Appendix 2. In Table 3 below, the list of simulations performed can be seen as well as data collected from the runs at apastron (furthest orbital distance) after the first passage of the star by the BH. Orbital jumps are unnecessary for many cases, necessary and appropriate for several, and necessary but not appropriate for the largest cases. For a complete list of simulations performed see Section 3.1 and Tables 3 and 4.

To implement orbital jumps, I need to make several small changes to the Starsmasher code. In the input file, I change the final time for the simulation to be a negative number, this tells the code to check for jump conditions. I also add a variable called RJUMP which determines the separation at which a jump will occur. I chose to set this distance in multiples of the tidal radius. To test the importance of the jump distance, I created two runs using an $80M_\odot$ BH with pericenter distances of 0.75 tidal radii, one with RJUMP equal to ten times the tidal radius (2688 $R_\odot$) and the other with RJUMP set to fifty times the tidal radius (13440 $R_\odot$). These simulations are still running, but when they are finished there will be a figure comparing the two runs.

An additional factor in jump runs is the common envelope mass and the ejected mass from the prior pass. For the two simulations discussed above, runs 15 and 17 as listed in Table 3, the mass that is bound to the BH is added to the mass of the BH when the orbital jump occurs and any unbound mass is removed. This is not an accurate representation of what happens as much of the bound mass does not accrete onto the BH. To address this, I set up another simulation, run 16, in which only 10% of the bound mass is added to the BH. To do this, I changed a variable in the file skipahead found in the Starsmasher src file called fkeep. By changing fkeep from 1 to 0.1 only 10% of the mass, energy, and momentum of the bound mass is added to the BH while the remaining 90% is thrown away.

2.3 Timestep

An important factor in maintaining the accuracy of the simulations is the timestep. The timestep is the amount of time that passes in the simulation between calculations for each particle. Decreasing the timestep results in higher accuracy but requires more computational power as more calculations are required for the same amount of simulation time. The timestep can be controlled by adjusting a series of constants denoted as Cn1 through Cn6. Cn1 through Cn4 have to do with interactions between sph particles that represent gas in the simulations. Cn1 is related to the signal speed around a particle, which is the sound speed with an additional contribution from artificial viscosity should that be present. Cn2 has to do with a particle's acceleration and the smoothing length *h*. Cn3 looks at the change in the internal energy of a particle. Cn4 relates to the signal speed as well as the acceleration of a particle relative to its surroundings, though I did not utilize Cn4 in my simulations. Cn5 and Cn6 look at interactions between particles and point masses, notably the BH particle and the core point of the RG in my simulations. Cn5 relates the velocity of a particle to the distance between the particle and the point mass while Cn6 does the same but for acceleration rather than velocity. For a more detailed explanation of Cn1 through Cn4 see Appendix A of Gaburov et al. (2010). The Cn values that I used for the majority of runs are as follows: Cn1 = 0.5, Cn2 = Cn3 = 0.06, and Cn5 = Cn6 = 0.02. Runs 3, 6, 9, and 12 used Cn5 = Cn6 = 0.005 as in those simulations energy conservation was violated by several percent. Lowering the value of Cn5 and Cn6 reduces the timescale which increases accuracy and improves energy conservation over the duration of a simulation. All of these values force the timestep to be small enough that a significant change cannot occur over the course of a single timestep as that would reduce the accuracy of the model which can be seen in a loss of energy conservation over time.

2.4 Post Processing: Splot

Starsmasher creates out files that contain data about every particle in the simulation at the time of the out file's creation. Throughout a simulation, thousands of out files are created. To interpret these data I use a program called Splot. Splot is a Fortran routine created by Dr. Jamie Lombardi that uses the out files created by Starsmasher to make a file called massAndMore.out.

This massAndMore file contains information such as the mass, position, spin, and energies of each body at various times throughout the simulation.

3. Results

3.1 Relaxation Used

For all dynamic simulations performed I used the same profile from the same relaxation run. The run that I found to be the most accurate representation of a $10M_{\odot}$ RG with a radius of $134.4R_{\odot}$ had the following inputs: final time 20000, the time between out files 20, number of particles 200000, equalmass 0, nnopt 250, hceiling 1344, hfloor 1, TRELAX 200, and TRELOFF 10000. Several plots of this relaxation can be seen in Figure 7 below. The red lines in the left half of Figure 7 shows expected values from MESA. Close adherence to those expected values is an indication that the relaxation is an accurate model of a RG star of this size and mass.

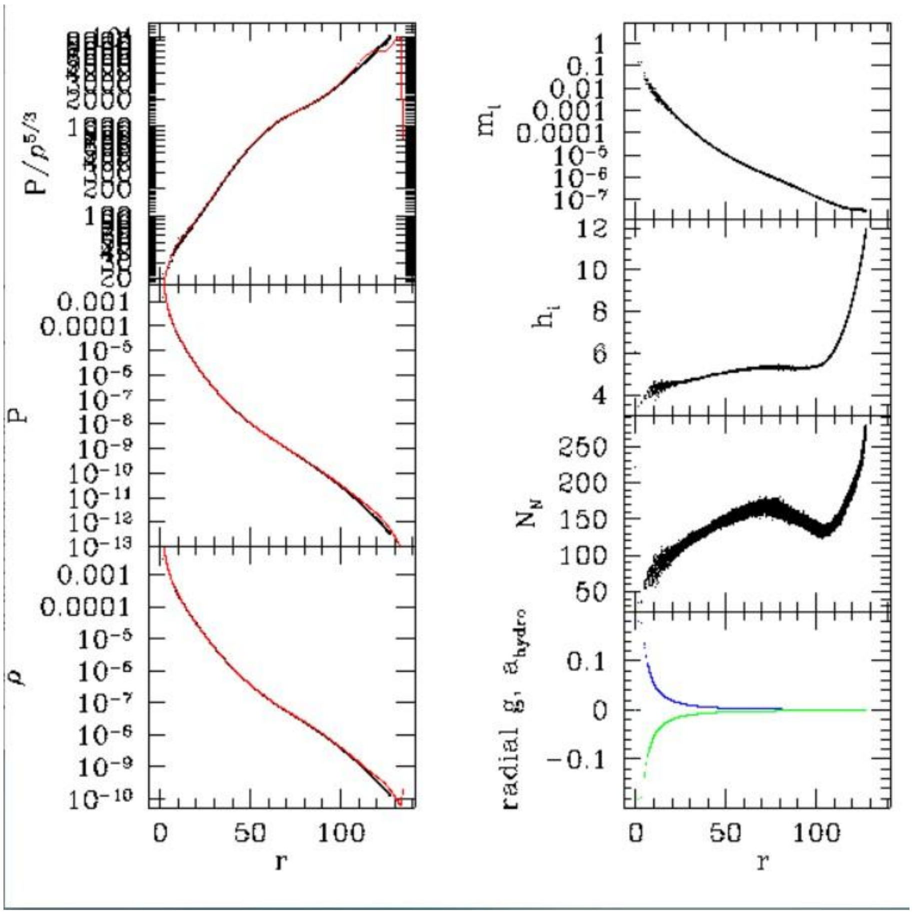

Figure 7. PA Plot from the relaxation used for dynamic simulations. On the left from bottom to top: density, pressure, pressure/density$^{5/3}$. On the right from top to bottom: mass, smoothing length, number of neighboring particles, and buoyancy and gravitational forces. Each point contains data from a specific particle from the relaxation. The horizontal axis is the radius of the star in solar radii. The red lines are expected values from the MESA model.

3.1 Simulations Performed

In Tables 3 and 4 below, information regarding the simulations performed can be found. Table 3 shows initial conditions as well as data after the first passage of the star by the BH. For runs in which only a single passage was performed, these measurements were taken once the star had reached a distance at which its mass was no longer changing. For runs in which multiple passages occurred, first-pass measurements were taken at apastron.

Number	MBH	M*	rp/R*	rp/rt	Sep0	MBHfp	M*fp	MCEfp	Orbital Period (years)	Num Orbits
1	10	10	0.25	0.25	1344.00	10.188	9.4312	0.03	0.17	4022
2	10	10	0.50	0.5	1344.00	10.021	9.881	0.005	2.58	162
3	10	10	0.50	0.5	1344.00	10.025	9.8828	0.005	2.57	958
4	10	10	0.75	0.75	1344.00	10.005	9.9655	0.0005	24.41	4601
5	20	10	0.31	0.25	1693.33	20.26	9.1885	0.05	0.33	212
6	20	10	0.31	0.25	1693.33	20.275	9.1853	0.041	0.33	290
7	20	10	0.63	0.5	1693.33	20.04	9.822	0.004	5.75	37
8	20	10	0.94	0.75	1693.33	20.012	9.948	0.0004	57.50	1
9	40	10	0.40	0.25	2133.47	40.3	8.87	0.03	0.75	244
10	40	10	0.79	0.5	2133.47	40.05	9.77	0.002	15.56	34
11	40	10	1.19	0.75	2133.47	40.017	9.933	0	163.41	1
12	80	10	0.50	0.25	2688.00	80.31	8.66	0.01	1.86	10
13	80	10	1.00	0.5	2688.00	80.064	9.729	0.001	46.51	1
14	80	10	1.50	0.75	2688.00	80.023	9.923	0.0002	258600	1
15	80	10	1.50	0.75	2688.00	80.023	9.923	0.0002	258600	11
16	80	10	1.50	0.75	2688.00	80.023	9.923	0.0002	258600	55
17	80	10	1.50	0.75	2688.00	80.023	9.923	0.0002	258600	1

Table 3: List of simulations performed. Columns 2-6 give initial conditions and columns 7-10 give values at the first apastron. The * character signifies information about the star. CE stands for the common envelope. All masses are in units of solar masses and distances are in solar radii. Runs 15, 16, and 17 performed jumps as described in section 2.2.4. Runs 3, 6, 9, and 12 used smaller Cn values as described in section 2.3.

Run Number	MBHf	M*f	MCE	ef	af	NumOrbits
1	10.197	3.125	0.635	0.484	3.105	4022
2	10.537	4.465	0.161	0.205	5.348	162
3	11.350	3.270	0.962	0.356	16.163	958
4	10.027	3.125	2.671	0.662	2.191	4601
5	20.450	3.706	0.293	0.289	33.913	212
6	21.327	3.997	0.000	0.445	42.047	290
7	20.427	5.607	0.251	0.739	306.836	37
8	20.012	9.948	0.000	0.987	9946.500	1
9	40.480	3.997	0.017	0.515	68.976	244
10	40.375	7.345	0.015	0.796	492.844	34
11	40.017	9.933	0.000	0.993	23664.600	1
12	80.761	4.603	0.022	0.841	336.999	10
13	80.064	9.729	0.001	0.989	12449.900	1
14	80.022	9.923	0.000	0.997	62094.100	1
15	80.093	9.841	0.001	0.995	36343.300	11
16	80.043	9.080	0.000	0.993	27694.700	55
17	80.019	9.922	0.001	0.997	62069.100	1

Table 4: List of simulations performed with final measurements. Columns from left to right: Run number, BH mass, star mass, common envelope mass, eccentricity, semimajor axis, number of orbits.

3.2 New Versions of Splot

As mentioned in Section 2.4, Splot is the post-processing code that I used to create massAndMore.out files which I used to create the various figures and tables presented. Over the course of my project, Lombardi and I used various iterations of Splot from Splot19 to Splot25 with each new version either containing new information of interest or improving ways in which Splot measured certain quantities. For example, Figures 8 and 9 below show the same information for Run 6. Figure 8 was made using the massAndMore generated by Splot24, notice that the eccentricity at late times covers a large range of values including several peaks where the eccentricity exceeded one. This on its own would not be problematic as it would not be unreasonable for a star to become unbound and be ejected from the system. However, if that were the case then the separation between the BH and RG would be increasing which is not so. This led Dr. Lombardi and I to believe that Splot24 was incorrectly calculating the eccentricity. In Splot25 the method for calculating eccentricity was changed to only include mass within each object's Roche lobe. The result of this change can be seen in Figure 9. Now the eccentricity at late times continues to decline which is consistent with the decreasing separation. This update also changed the value of eccentricity for the other simulations but to a lesser degree. All results that refer to eccentricity throughout the rest of this paper used Splot25.

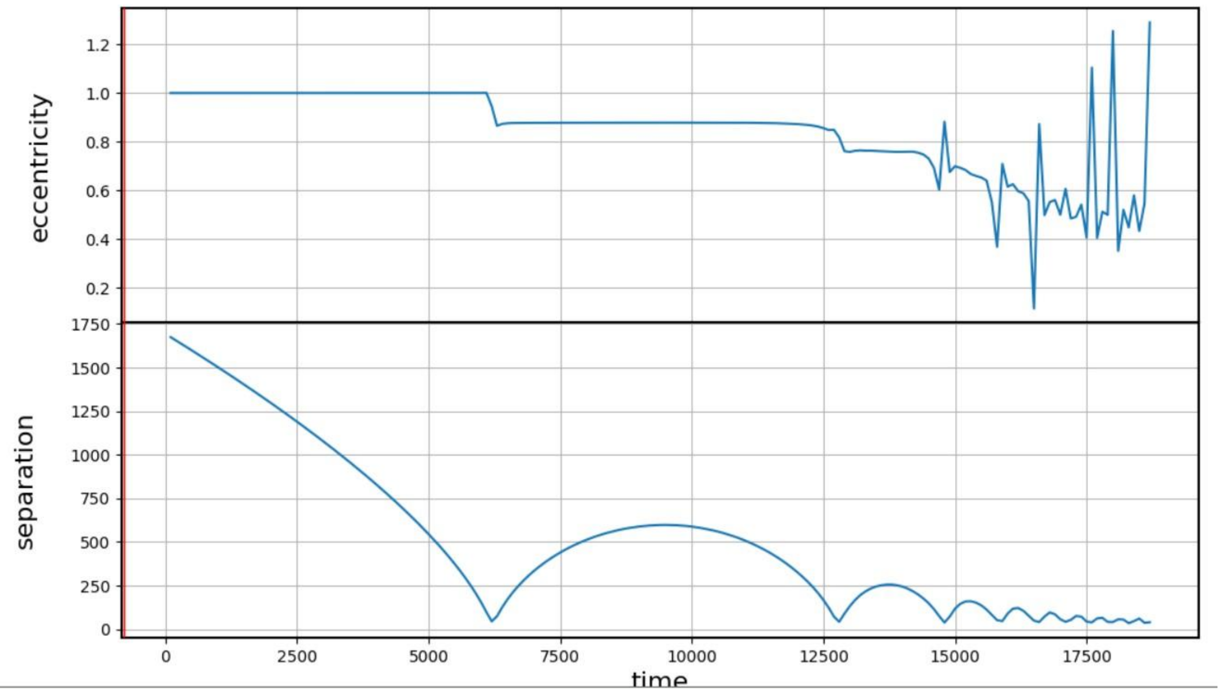

Figure 8: Eccentricity and Separation vs Time for Run 6 Splot24. The erratic eccentricity combined with decreasing separation led me to believe that eccentricity was being incorrectly calculated.

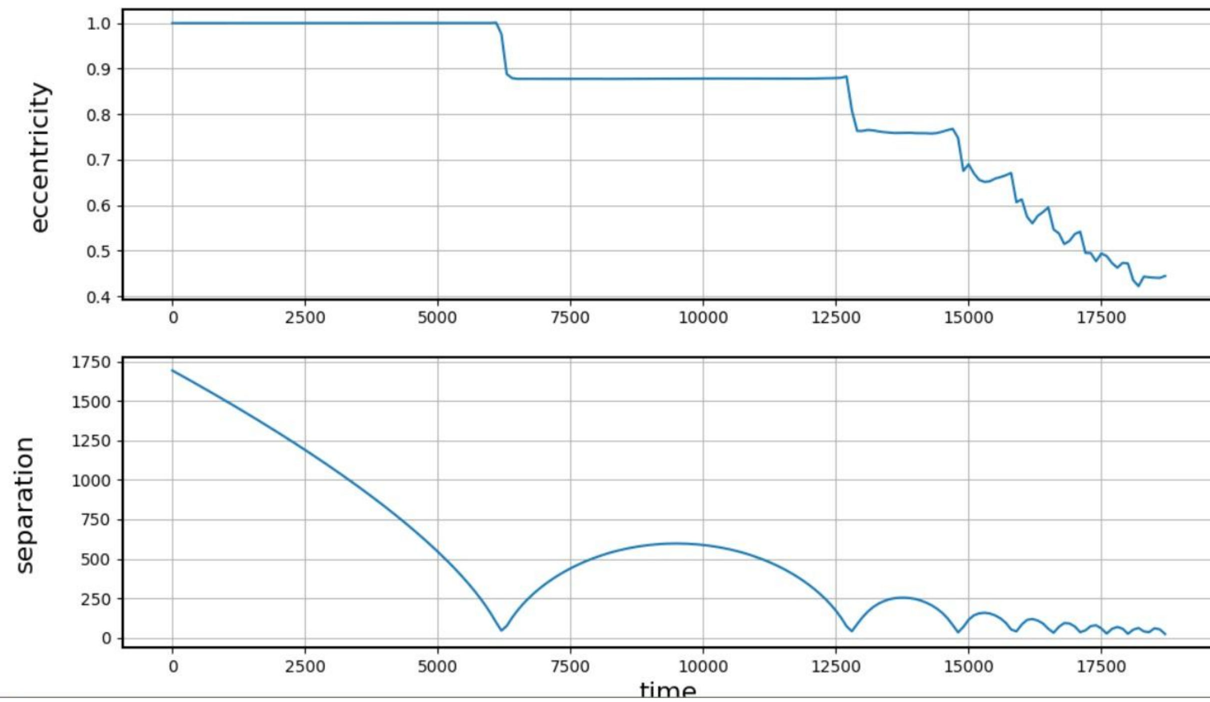

Figure 9: Eccentricity and Separation vs Time for Run 6 Splot25. After updating the Splot routine the eccentricity shown is more consistent with the change in separation at late times.

3.3 The Effect of Timestep

As discussed in section 2.3, the timestep can be adjusted using the Cn constants. To demonstrate this, I conducted two simulations that are identical except for the values of Cn5 and Cn6. I chose to change these Cn values as, by examining the log.sph files from Run 5, I could see that the gas-point mass time steps were more significant than that of the gas-gas interactions. In Figures 10 and 11 below the energy values for Runs 5 and 6 can be seen respectively. In Run 5 energy conservation was violated by about 1% while in Run 6 energy conservation was violated by less than 0.5%. This increase in accuracy came at the expense of computational time, the time between out files in Run 5 was about twenty minutes while Run 6 took about an hour between out files. Halving the error tripled the computation time.

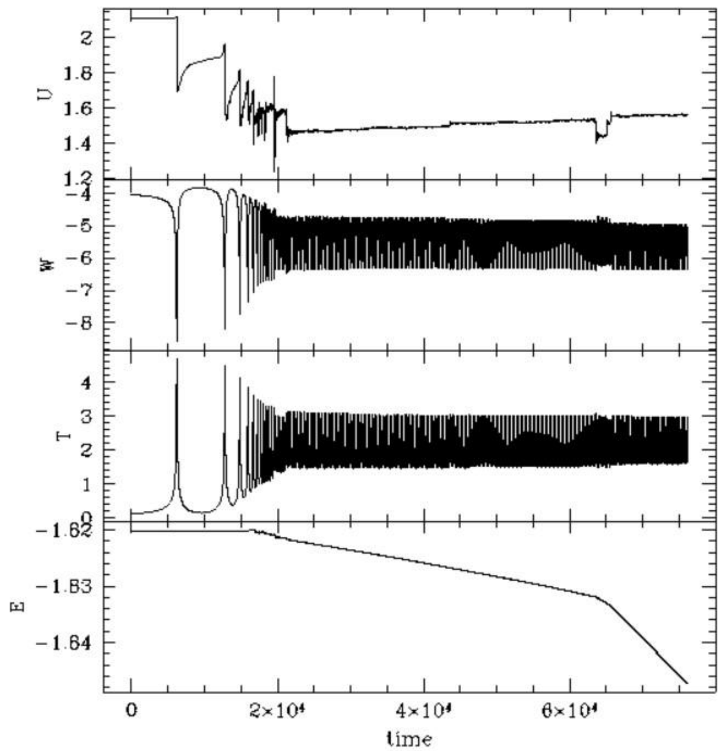

Figure 10: Run 5 from Table 3. This run used cn1 = 0 .5, cn2 = cn3 = 0.06, and cn5 = cn6 = 0.02. The graphs show from top to bottom: internal energy *U*, gravitational potential energy *W*, kinetic energy *T*, and total energy *E*. Note that energy conservation is violated by approximately 1%. Energies are given in code units, see Section 2.2 for conversion details. This Figure was created using Splash (Price 2007).

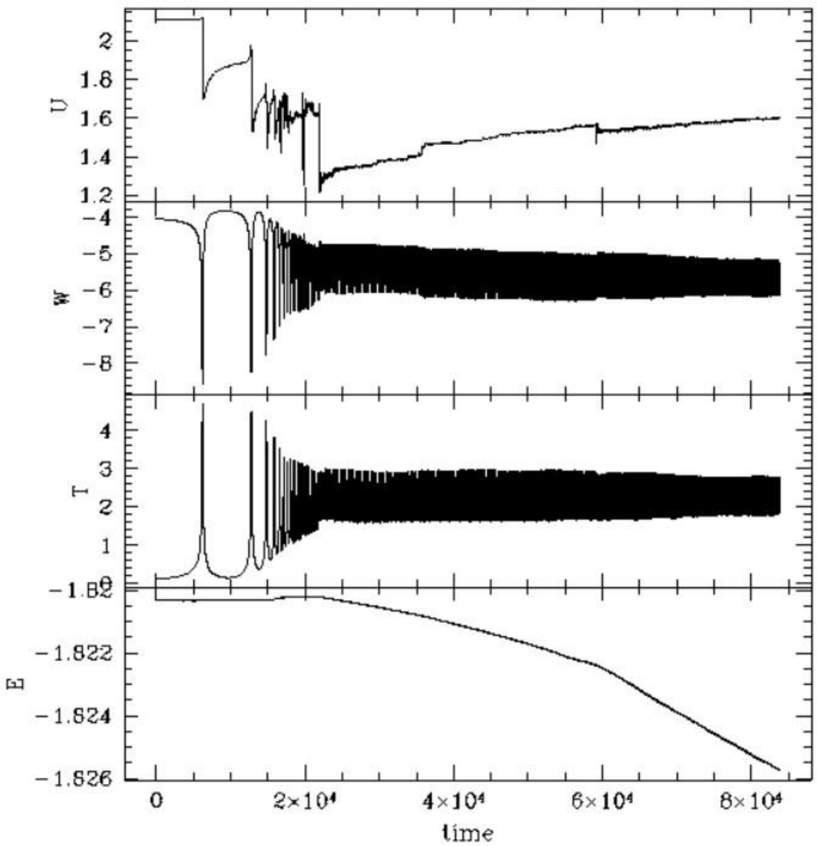

Figure 11: Run 6 from Table 3. This run used cn1 = 0.5, cn2 = cn3 = 0.06, and cn5 = cn6 = 0.005. Other than the changed values for cn4 and cn5 this run was identical to run 5. Notice that energy conservation is only violated by less than 0.5% over a longer total time. Energies are given in code units, see Section 2.2 for conversion details. This Figure was created using Splash (Price 2007).

3.4 The Long Run

One run worth discussing in greater depth is run 4 in which a $10M_{\odot}$ BH collides with an RG of equal mass with a periastron distance of 0.75 times the tidal radius. This run was allowed to run for much longer than the other runs, approximately 5 months after accounting for several brief interruptions. This amounted to over one and a half million iterations. The energy graphs for this run can be seen below in Figure 12. Each dip in gravitational potential energy has a corresponding spike in kinetic energy which corresponds to a passage of the star by the periastron distance. The decreasing magnitude of these spikes signifies a circularization of the orbit that can also be seen in the decrease in eccentricity shown in Figure 13 and Figure 14. After a time of $4.9 * 10^6$ the separation between the point masses that represent the core of the RG and the BH becomes less than twice their respective smoothing lengths, about $6R_\odot$ for each. This leads to inaccuracies in the gravitational calculations and corresponds to the sudden changes in energy and eccentricity seen in Figures 12, 13, and 14 at that time.

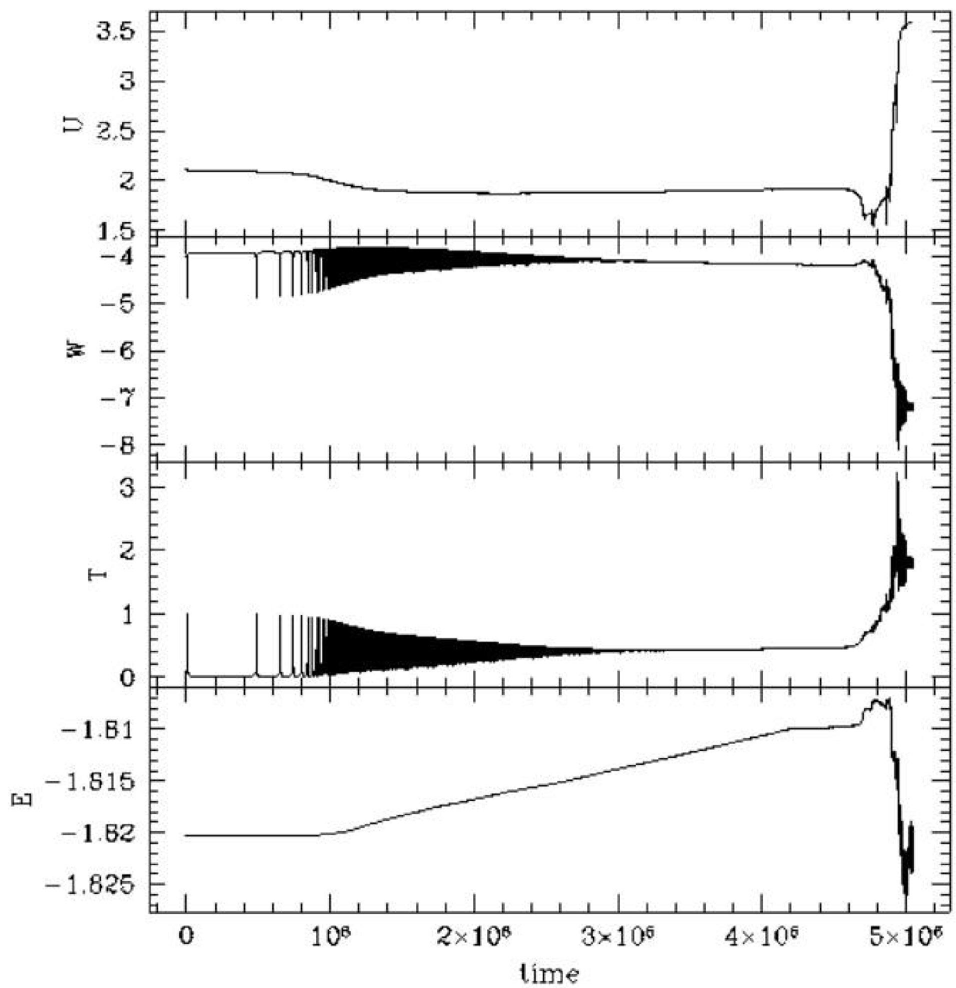

Figure 12: Run 4 allowed to go to very late times. Graphs show, from top to bottom, internal energy, gravitational potential energy, kinetic energy, and total energy all in code units that are defined in Section 2.2.. Notice the change in slope of the total energy around $t = 4 * 10^6$ this shows where the run was stopped and restarted using smaller Cn values to preserve energy conservation. This Figure was created using Splash (Price 2007).

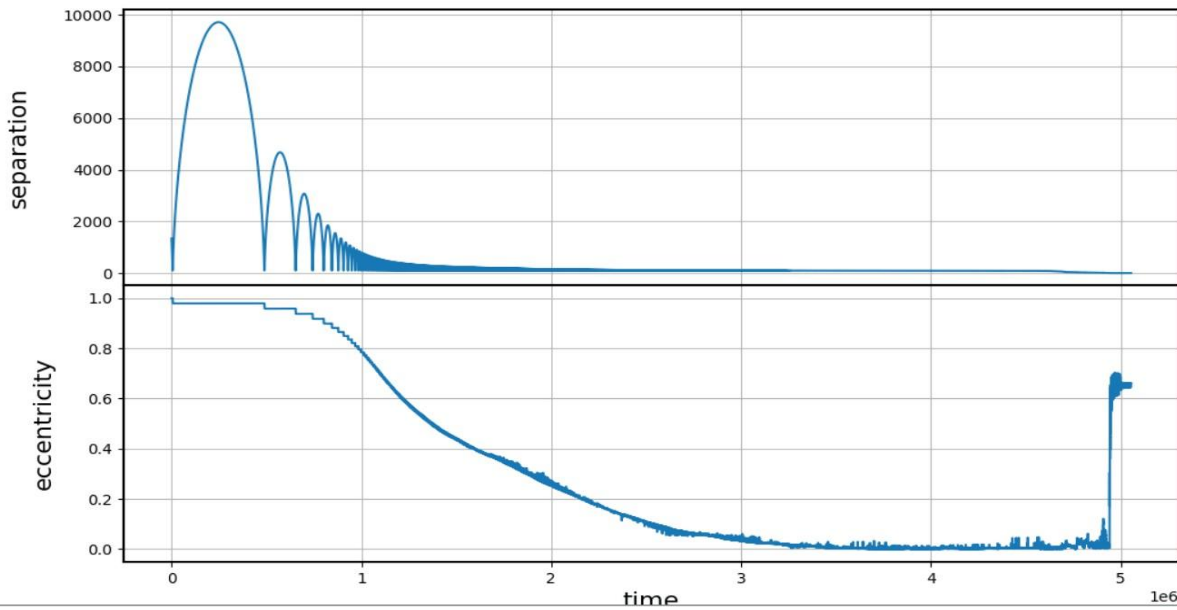

Figure 13: Run 4 Eccentricity and Separation Data. The time axis is in code units, separation is in solar radii, and the orbital period is in code time units. For a discussion of code units see Section 2.2.

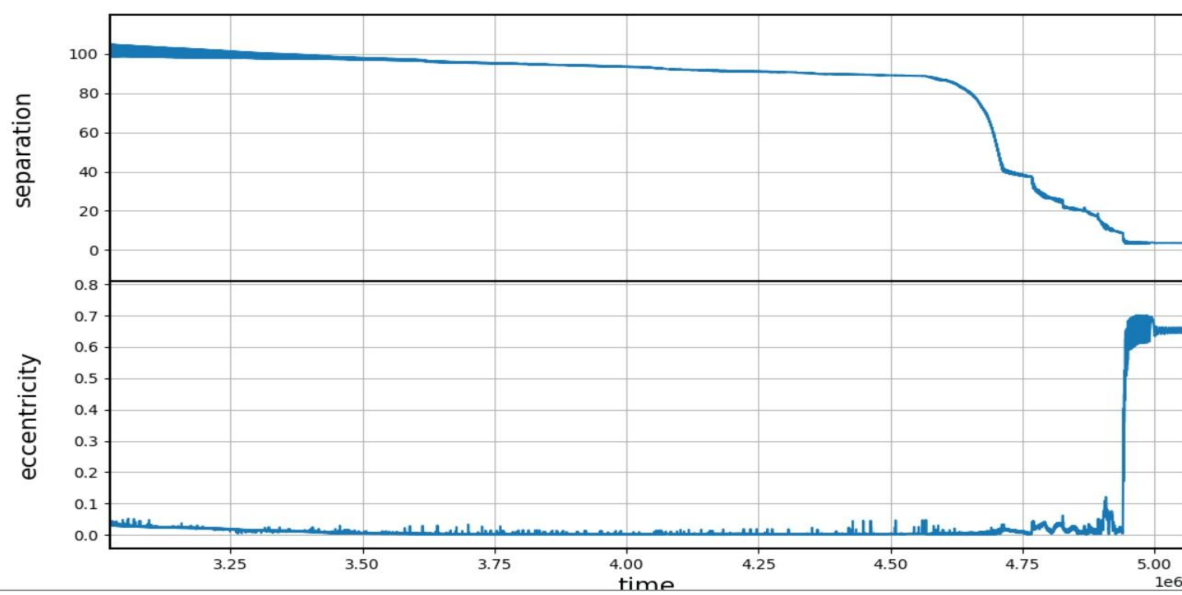

Figure 14: Run 4 Eccentricity and Separation at Late Times. The time axis is in code units, separation is in solar radii, and the orbital period is in code time units. For a discussion of code units see Section 2.2.

The eccentricities shown in Figure 14 above appear erratic because of their scale. The jumps that appear in the figure before the core particles are within the gravitational smoothing length are small enough to be lingering issues with Splot25. I encountered similar larger effects with previous iterations of Splot. After a time of $4.7 * 10^6$ the separation goes from a steep decline to a more stuttered change. This is likely due to the low number of particles involved around the core of the RG which continue to be stripped from the star discretely. In reality, this decrease in mass would be more continuous and is sometimes referred to as the plunge-in of the star.

Worth further discussion is the change in internal energy during Run 4 as seen in Figure 12. The internal energy decreases over the first several dozen passages as the star loses mass leading to the gas expanding and cooling down. Then the internal energy remains nearly constant with small changes for a long period during which mass is slowly lost from the star as can be seen in the long flat region of the top portion of Figure 15. At late times the internal energy begins to increase which could be due to the stripping of additional matter from the star at this time. Most of that mass becomes unbound, except for about half of a solar mass which becomes temporarily bound to the BH. The mass bound to the star, the mass bound to the BH, and the unbound mass can be seen below in Figure 15. The mass of the RG never falls below the mass of the core point which is 3.125 $M_{\odot}$.

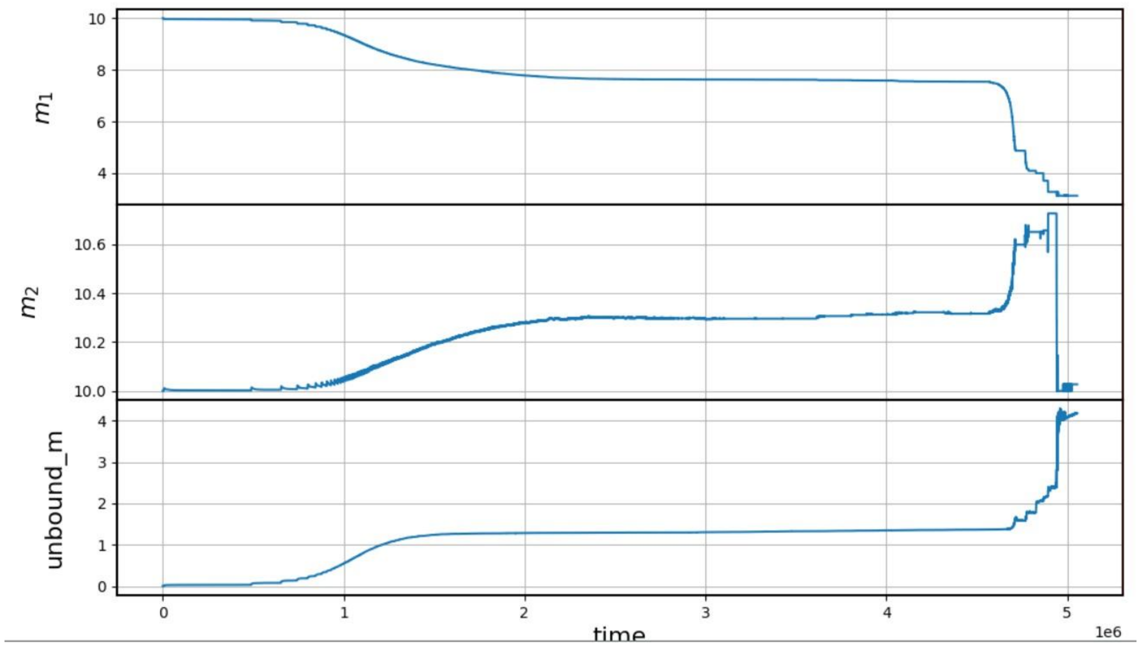

Figure 15: RG Mass vs Time for Run 4. Here *m1* is the mass of the star, *m2* is the mass of the BH and *unbound_m* is the mass that is not gravitationally bound to either. Note that the time axis is in units of code time units. For a discussion of code units see Section 2.2. The abrupt decreases in mass correspond to passages of the star through periastron by the BH.

The change in mass shown in Figure 15 at early times mirrors the change in internal energy shown at the top of Figure 12. Starting around a time of $2*10^6$, which corresponds to $3.8 * 10^4$ days, the internal energy begins to increase while the mass continues to gradually decrease.

At late times, beginning around $5.5*10^5$ days, the BH and RG form a contact binary as pictured in Figure 16a below. This leads to the total destruction of the star which is mirrored in the mass of the star in Figure 15 decreasing rapidly at this time. This contact binary stage lasts for tens of thousands of days with the separation of the binary gradually decreasing and mass being knockout out of the system. Figure 16b shows the system near the end of the contact binary stage.

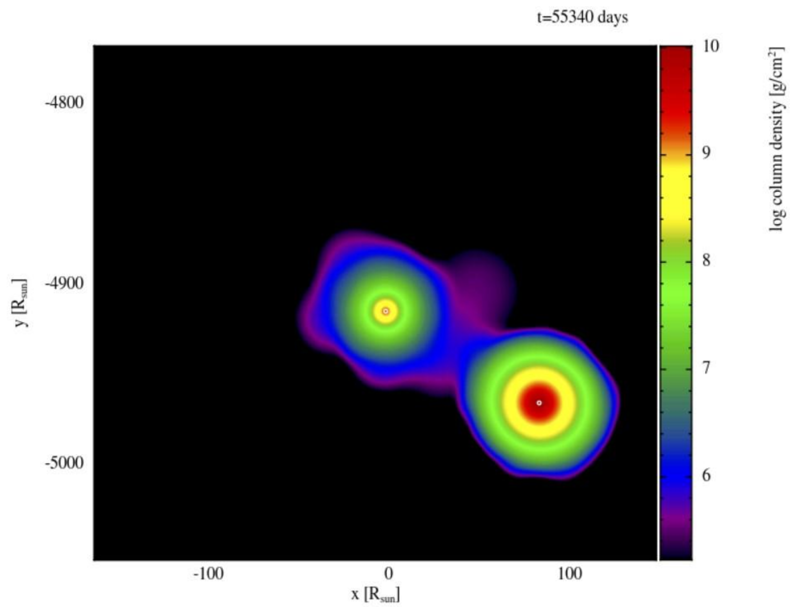

Figure 16a. The column density of the BH-RG binary shortly after becoming a contact binary. The object on the right is the star with the core point resting at its center.

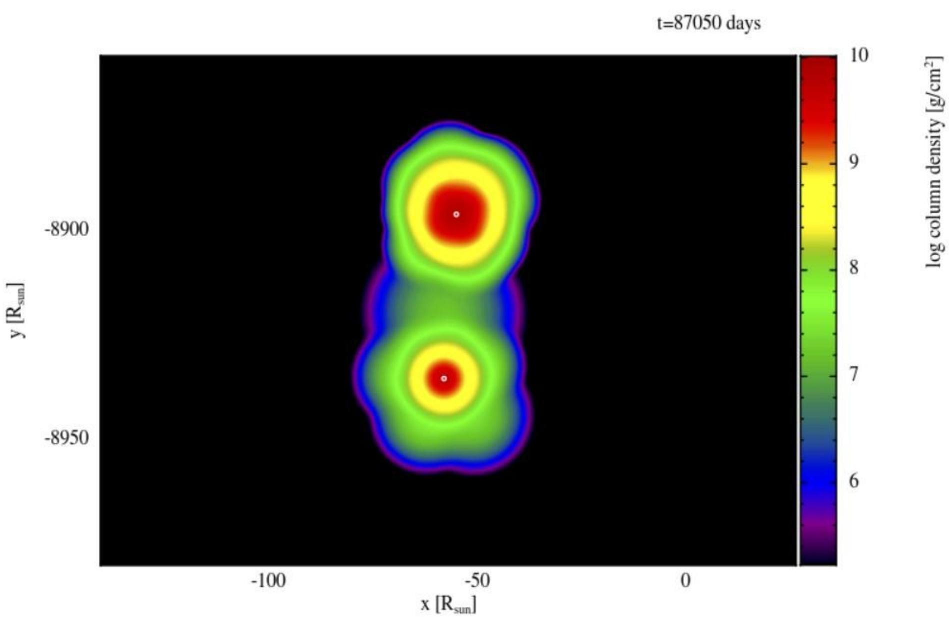

Figure 16b. The contact binary. As mass has continued to be transferred from the RG to the BH the column density of the two objects has become more similar.

After this point in the simulation, some of the limitations of Starsmasher begin to reveal themselves. As the last of the star's envelope is stripped the particle aspect of the simulation becomes problematic. Recall that Starsmasher uses a hexagonal lattice of particles to model the star with a single core particle at the center. The core particle becomes gravitationally bound to the BH and the six particles that originally surrounded the core particle are ejected. Below in Figure 17, these individual particles can be seen as regions of higher density. All six are present with two of them being bound to the BH and core particle near the center of the image. At this point in the simulation, the resolution is inadequate to have much confidence in the specific results.

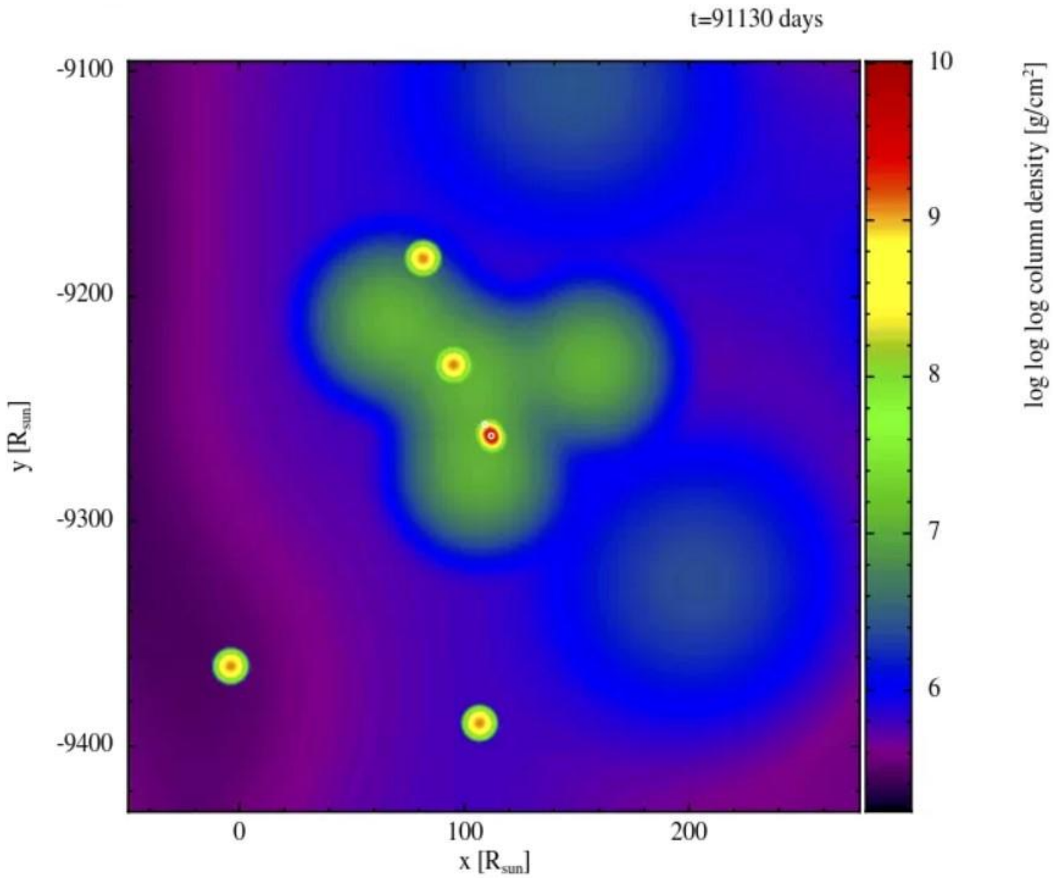

Figure 17. Column density reveals the limitations of the simulation. The BH particle and the core particle from the RG occupy the region with the highest density along with two of the six particles that originally surrounded the core particle of the RG. The remaining four make up the four other high-density regions depicted.

This system would likely result in a merger of the core and BH but that goes beyond the capabilities of this simulation. After the time shown in Figure 17, the core point of the star and the BH remain in orbit around each other and continue to meander through the loose mass in the system. The point masses each have a smoothing length of approximately six solar radii around them so once they get within twelve solar radii of each other gravitational smoothing reduces the accuracy of any calculations performed around them.

3.5 Collective Data

3.5.1 First Pass Mass

The mass of the RG after its first passage can be seen in Figure 18 below. For simulations that completed multiple orbits, the mass is measured at the apastron distance. For simulations that completed only a single orbit and simulations that used orbital jumps, the mass is measured at the end of the simulation and at the jump distance respectively. In the simulations with larger ratios of periastron distance to the tidal radius ($\frac{r_p}{r_t}$) the RG lost less mass compared to lower $\frac{r_p}{r_t}$ simulations. Additionally, as the mass of the BH increased so to did the mass lost after the first pass. Interestingly, the difference in mass loss due to the increasing mass of the BH decreases as $\frac{r_p}{r_t}$ increases.

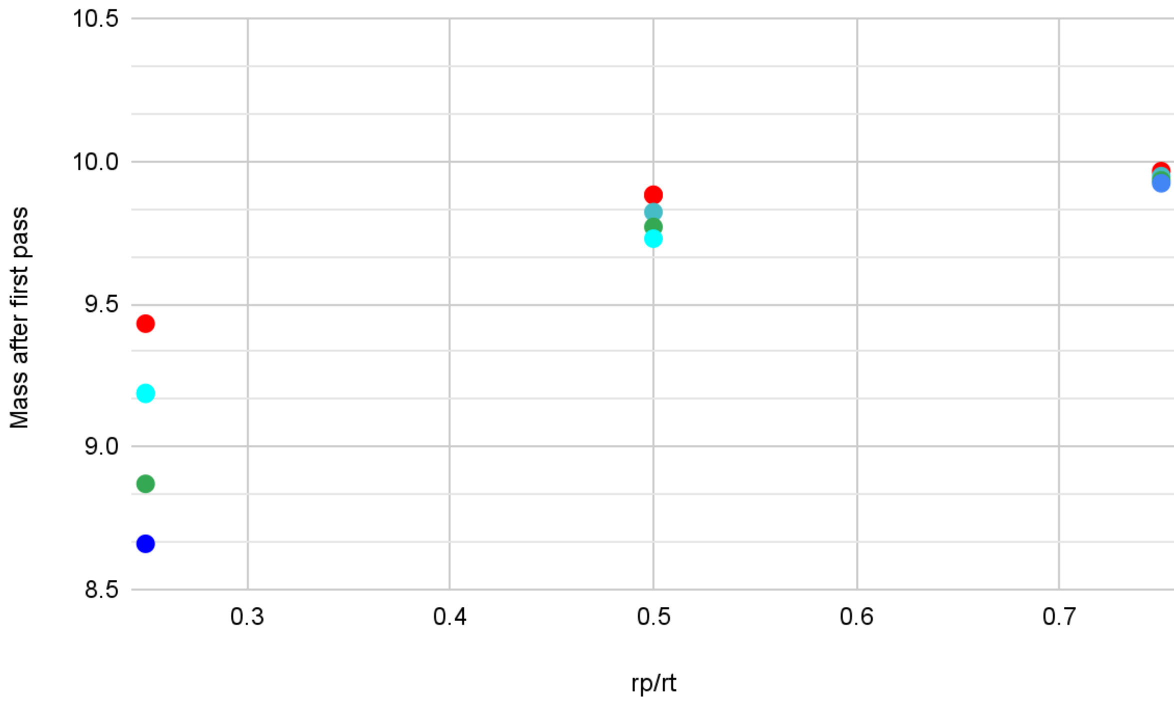

Figure 18: The star's mass after its first passage by the BH vs the ratio between pericenter distance r_p and the tidal radius r_t. The color of the dot indicates the mass of the BH with red being a $10M_\odot$, teal being $20M_\odot$, green $40M_\odot$, and blue $80M_\odot$.

In looking for an explanation for why that might be the case, I first consider how the tidal force changes with r_p. By setting $r = r_p = Cr_t$ in Equation 3, where C is a constant which varies from run to run between 0.25 and 0.75 as listed in column 5 of Table 3, and plugging in the formula for r_t given in Equation 4 I find that

$$F_t = \frac{-2M_*}{C^3R^2} \quad (11).$$

The problem with Equation 11 is that there is no dependence on the M_{BH} and there should be some relationship between M_{BH} and the first pass mass loss. Dr. Lombardi had the idea that perhaps the change could be found in the amount of time that the star spends experiencing a tidal force strong enough to cause mass loss. Through some mathematical manipulation, we find that the time amount of time that the star spends under forces that could cause tidal disruption is

$$t_{dis} \approx C(1 - C)^{1/2}(\frac{R^3}{GM_*(1+\frac{M_*}{M_{BH}})})^{1/2}, \qquad (12)$$

Where C is the same constant in Equation 11. For a complete derivation of this see Appendix 3. If we assume that mass loss is proportional to the displacement time and remove the constants this leads:

$$\Delta M \propto (1 + \frac{M_*}{M_{BH}})^P \qquad (13)$$

Where $\Delta M$is the change in mass after the first pass. The exponent P in Equation 13 is left as a variable rather than the value $\frac{-1}{2}$ that it holds in Equation 12 because there is a more accurate way to determine the value of P that the series of assumptions that were made to approximate t_{dis}. By taking the logarithm of both sides of Equation 13 I get

$$log(\Delta M) \propto P * log(1 + \frac{M_*}{M_{BH}}) + C, \qquad (14)$$

where C is some constant. Because I have values for ΔM I can plot this. The equations of the resulting lines will show the value of P and C. This data can be seen in Figure 19 below.

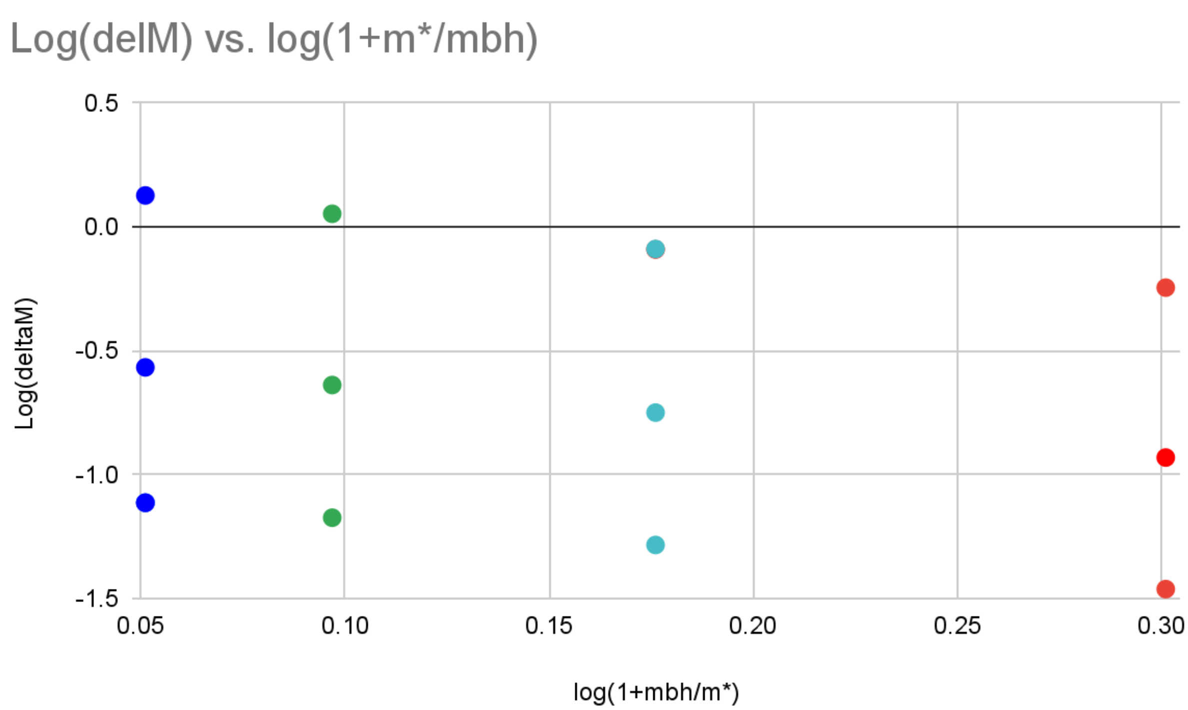

Figure 19. Log(ΔM) vs Log($1 + \frac{M_*}{M_{BH}}$). The color of the dot indicates the mass of the BH with red being a $10M_\odot$, teal being $20M_\odot$, green $40M_\odot$, and blue $80M_\odot$. The higher values of $\frac{r_p}{r_t}$ correspond to lower Log(ΔM) in all cases.

The data in Figure 19 forms nearly linear relationships between points of constant $\frac{r_p}{r_t}$. Different values of $\frac{r_p}{r_t}$ do not have quite the same slopes but they are similar with the $\frac{r_p}{r_t} = 0.25$ case having a slope of -1.5, the $\frac{r_p}{r_t} = 0.50$ case having a slope of -1.45, and the $\frac{r_p}{r_t} = 0.75$ case having a slope of -1.4.

3.5.2 Zeta

As mentioned in section 1.8, ζ is a constant involved in the mass lost by the star in its first pass by the BH. Kiroglu et al. found ζ to be ~5.6 for interactions between main sequence stars and intermediate-mass BH (2022). The value of ζ for my runs can be seen below in Table 5. As can be seen, the value varies from run to run between 0.96 and 3.77. As the mass of the BH increases ζ tends to increase and as the periastron distance increases ζ tends to increase as well. This shows that the relationship found in Kiroglu et al. 2022 only holds for the situation in their paper and not for RG-Stellar mass BH interactions.

Number	zeta
1	0.96
2	1.61
3	1.58
4	2.22
5	1.47
6	1.47
7	2.34
8	2.86
9	2.22
10	2.95
11	3.40
12	2.78
13	3.52
14	3.77
15	3.77
16	3.77
17	3.77

Table 5: Zeta. Run numbers and zeta. The last four runs are identical until after the first pass so they have identical zeta values. The formula to find zeta can be found in section 1.8. Zeta is related to the mass lost by the star in its first passage by the BH.

4 Discussion

This project found that the mass lost by a RG star in a TDE event with a BH is affected by the mass of the star and the periastron distance. Decreasing periastron distance and increasing BH mass both increase the mass lost by the star. The mass loss does not follow the same relationship found in Kiroglu et al. 2022. Further work worth pursuing could include additional ratios between periastron distance and the tidal radius or using giant stars of different masses. At late times, the resolution of the simulations is inadequate so perhaps later studies could perform simulations using more particles or with smaller timesteps. Treating the BH as a point mass is useful for simplifying the simulation but results in a BH that cannot accrete matter. I did not study the common envelope evolution in depth. The state of the common envelope is relevant to the electromagnetic radiation created in the types of interactions modeled, so further study in this area could be useful in identifying this type of interaction when it occurs in nature. A limitation of this project was my inability to study every run in depth. It would be worthwhile to examine more of these simulations after running them longer to see if they have plunge-ins similar to the one discussed in section 3.4. If not every simulation experiences a plunge-in, it would be interesting to see which ones did and which ones did not. The case studied here, a $10M_\odot$ RG with various mass BHs, is only one small piece of the parameter space. A potential future project could simulate RGs of smaller mass, perhaps $1M_\odot$ or $2M_\odot$, as these smaller stars would be more common in the later stages of globular cluster evolution (see Figure 2).

Appendix 1 Schwarzschild Radius

To find the escape velocity of a system, let us use energy conservation. As a reminder

$$E = K + U$$

where K is the kinetic energy given by

$$K = \frac{1}{2}mv^2,$$

U is the gravitational potential energy given by

$$U = \frac{GMm}{R},$$

and energy conservation tells us that

$$E_i = E_f.$$

Now, image a test mass m_1 on a planet of mass M and radius R. For the test mass to escape the gravity of the planet, it must reach a final state in which the gravitational potential energy from the planet on the mass is 0 and so is the mass's velocity. In short

$$U_f = 0,\ K_f = 0,\ E_f = 0.$$

From energy conservation we can say:

$$E_f = 0 = E_i = \frac{1}{2}m_1 v_e^2 - \frac{Gm_1 M}{R},$$

and thus

$$\frac{1}{2}m_1 v_e^2 = \frac{Gm_1 M}{R}.$$

Solving for v_i gives

$$v_e = \sqrt{\frac{2GM}{R}},$$

which is the escape velocity.

The Schwarzschild radius is the distance from a black hole at which $V_e = c$ where c is the speed of light. By rearranging the above equation to solve for r we get

$$Schwarzschild\ Radius = R_S = \frac{2GM}{c^2}$$

Appendix 2 Thermal Timescale

The thermal timescale, also known as the Kelvin-Helmholtz timescale, is defined as the amount of time that it would take for the star to radiate away all of its gravitational energy in the form of light. To put it mathematically

$$T_{thermal} = \frac{E}{L}.$$

From the Starsmasher energy file from the relaxation run for the 10M$_\odot$ RG, I find the internal energy of the star to be 2.11 code units. To convert code units to joules, this must be multiplied by $\frac{GM_\odot^{\ 2}}{R_\odot}$, where $G = 6.67 * 10^{-11}\frac{Nm^2}{kg^2}$, $M_\odot = 1.981 * 10^{30}kg$, and $R_\odot = 6.955 * 10^8$. This gives an approximate energy of $E \approx 8 * 10^{41}$ joules. The luminosity of the same star can be found in the profile file and has the value $L = 2.0875 * 10^4 L_\odot$. Where $L_\odot = 3.8 * 10^{26}$ joules per second. Which gives $L \approx 7.6 * 10^{30}$joules per second. By plugging these values into the above equation I get

$$T_{thermal} \approx 10^{11} seconds \approx 3000\ years.$$

This approximation only accounts for the envelope of the star due to Starsmasher treating the core of the RG as a point mass. If I fully simulated the core of the star, the internal energy would be significantly larger, potentially by several orders of magnitude. However, I am using this timescale as the upper limit at which orbital jumps will be performed so I will not be performing jumps when they are not applicable.

Additionally, this timescale will change after each pass of the star by the BH. The TDE will increase the luminosity of the star which in turn shortens the thermal timescale. There is much room for improvement in this approximation method.

The values of constants were found in Carrol and Ostlie 2018.

Appendix 3: Disruption Time t_{dis}

This will be an approximation that disregards constants of order unity and is intended to give a ballpark estimate with the correct proportionalities. A star can be disrupted while it is within one tidal radius of the BH. As such,

$$t_{dis} \approx (\frac{r_t}{r^{**}})^{1/2},$$

where r^{**} is the second time derivative or r.

To find r^{**} I use Equation 8.18 from Thornton and Marion 2004:

$$\mu(r^{**} - r\theta^{*2}) = F(r), \qquad (8.18)$$

where μ is the reduced mass, in this case $\frac{M_{BH}M_*}{M_{BH}+M_*}$, and θ^* is the rate of change of the angular position of the star relative to the BH. For the sake of simplicity, I will be looking at the orbit at periastron which makes $\theta^* = r_p v_p$, where v_p is the velocity of the star at periastron.

Using conservation of energy and the fact that the system began as a parabolic orbit (which makes the initial total energy zero), I can find v_p by the following:

$$\frac{1}{2}\mu v_p^{\ 2} - \frac{G\mu M}{r_p} = 0,$$

where M is the sum of M_{BH} and M_*. This leads to

$$v_p = \sqrt{\frac{2GM}{r_p}},$$

$$\theta^* = \sqrt{\frac{2GM}{r_p^{\ 3}}}.$$

Plug that into 8.18 and solve for r^{**}

$$r^{**} = r_p(\frac{2GM}{r_p^{\ 3}}) - \frac{GM}{r_P^{\ 2}} = \frac{GM}{r_p^{\ 2}}$$

Plug this into the original equation for t_{dis} and include that $r_p = Cr_t$:

$$t_{dis} \approx \left(\frac{2r_t - Cr_t}{GM} r_p^{\,2}\right)^{1/2} = C(1 - C)^{1/2}\left(\frac{r_t^{\,3}}{GM}\right)^{1/2}.$$

This assumes that there is no mass loss outside of the tidal radius. Plug in Equation 4 for r_t.

$$t_{dis} \approx C(1 - C)^{1/2}\left(\frac{R^3 M_{BH}}{GM_*(M_{BH} + M_*)}\right)^{1/2} = C(1 - C)^{1/2}\left(\frac{R^3}{GM_*(1 + \frac{M_*}{M_{BH}})}\right)^{1/2}$$

As previously mentioned, this is a rough approximation. However, the C relationship and the $\frac{M_*}{M_{BH}}$ in the denominator seem to be correct.

Works Cited

Alexander, T. (2017). *Stellar Dynamics and stellar phenomena near a massive black hole ...* Annual Review of Astronomy and Astrophysics. Retrieved November 6, 2022, from https://www.annualreviews.org/doi/10.1146/annurev-astro-091916-055306

Ballone, A., Costa, G., Mapelli, M., MacLeod, M., Torniamenti, S., & Manuel, J. (2022). Formation of black holes in the pair-instability mass gap: Hydrodynamical simulations of a head-on massive star collision. *ArXiv*. https://doi.org/10.1093/mnras/stac3752

B. W. Carroll and D. A. Ostlie, An Introduction to Modern Astrophysics, Cambridge University Text, 2018.

Fogarty, S. "Mass Loss in Hyperbolic Collisions Between Stars and Black Holes". Senior Project, Allegheny College, November 2021

Gaburov, Evghenii, et al. "On the Onset of Runaway Stellar Collisions in Dense Star Clusters - II. Hydrodynamics of Three-Body Interactions." *NASA/ADS*, Feb. 2010, https://ui.adsabs.harvard.edu/abs/2010MNRAS.402..105G/.

Guillochon, J. (2012). Hydrodynamical Simulations to Determine the Feeding Rate of Black Holes by the Tidal Disruption of Stars: The Importance of the Impact Parameter and Stellar Structure. *ArXiv*. https://doi.org/10.1088/0004-637X/767/1/25

Hatfull, R. W., Ivanova, N., & Lombardi Jr, J. C. (2021). Simulating a stellar contact binary merger -- I. Stellar models. *ArXiv*. https://doi.org/10.1093/mnras/stab2140

Kyle Kremer, James C. Lombardi, Jr., Wenbin Lu, Anthony L. Piro, & Frederic A. Rasio (2022). Hydrodynamics of Collisions and Close Encounters between Stellar Black Holes and Main-sequence Stars. *ArXiv*. https://arxiv.org/abs/2201.12368

Kıroğlu, Fulya, private communication. 2022

Kıroğlu, Fulya, private communication. 2023

Kıroğlu, F., Lombardi Jr., J. C., Kremer, K., Fragione, G., Fogarty, S., & Rasio, F. A. (2022, October 14). *Tidal disruption of main-sequence stars by intermediate-mass Black Holes*. arXiv.org. Retrieved December 5, 2022, from https://arxiv.org/abs/2210.08002

Law-Smith, J., Guillochon, J., & Ramirez-Ruiz, E. 2019, ApJL, 882, L25, doi: 10.3847/2041-8213/ab379a

Lombardi, James, "Dealing With SPH Codes," in *Kavli Institute for Theoretical Physics*, Santa Barbara, 2017

Paxton, B., Bildsten, L., Dotter, A., Herwig, F., Lesaffre, P., & Timmes, F. (2011). *Modules for experiments in Stellar astrophysics (MESA)*. NASA/ADS. Retrieved October 15, 2022, from https://ui.adsabs.harvard.edu/abs/2011ApJS..192....3P/abstract

Price, D. J., & Monaghan, J. J. (2006, October 30). *An energy-conserving formalism for adaptive gravitational force softening in SPH and N-body codes*. arXiv.org. Retrieved April 3, 2023, from https://arxiv.org/abs/astro-ph/0610872v1#

Rosswog, S. (2009). Astrophysical Smooth Particle Hydrodynamics. *arXiv*. https://doi.org/10.1016/j.newar.2009.08.007

Ryu, T., Perna, R., & Wang, Y. 2022, arXiv e-prints, arXiv:2206.00603. https://arxiv.org/abs/2206.00603

S. Karekal, R. Das, L. Mosse and P. W. Cleary, "Application of a mesh-free continuum method for simulation of rock caving processes," *International Journal of Rock Mechanics and Mining Sciences,* vol. 48, no. 5, 2011.

Thornton, S. T., & Marion, J. B. (2004). *Classical dynamics of particles and systems*. Brooks/Cole.

Tran, Jacky. “Modeling Tidal Disruption Encounters and Analysis with a Data Visualization Tool - Hypermongo.” Senior Project, Allegheny College, December 2022